NASA CR134989

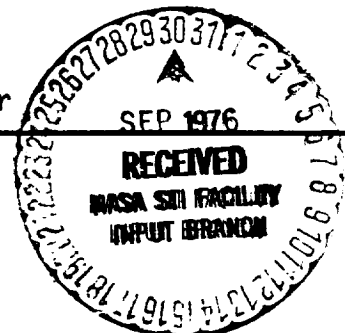# SOME WEAR STUDIES ON AIRCRAFT BRAKE SYSTEMS

TING-LONG HO

TRIBOLOGY LABORATORY
DEPARTMENT OF MECHANICAL ENGINEERING,
AERONAUTICAL ENGINEERING & MECHANICS
RENSSELAER POLYTECHNIC INSTITUTE
TROY, NEW YORK 12181

OCTOBER 1975

Prepared for

AEROSPACE SAFETY RESEARCH AND DATA INSTITUTE
LEWIS RESEARCH CENTER
NATIONAL AERONAUTICS AND SPACE ADMINISTRATION
CLEVELAND, OHIO 44135

Under

1. Report No. NASA CR 134923	2. Government Accession No.	3. Recipient's Catalog No.
4. Title and Subtitle Some Wear Studies on Aircraft Brake Systems		5. Report Date October 1975
		6. Performing Organization Code
7. Author(s) Ting-Long Ho		8. Performing Organization Report No.
		10. Work Unit No.
9. Performing Organization Name and Address Rensselaer Polytechnic Institute Troy, New York 12181		11. Contract or Grant No. NGR 33-018-152
		13. Type of Report and Period Covered Contractor Report
12. Sponsoring Agency Name and Address National Aeronautics and Space Administration Washington, D.C. 20546		14. Sponsoring Agency Code

16. Abstract

An initial investigation of both worn surfaces of friction pads and steel rotors which are being applied in current aircraft brakes has been carried out by employing electron microprobe and x-ray diffraction analysis. It consists of the topographical study and the analysis of chemical element distribution.

Based upon this initial examination, two approaches, microscopic and macroscopic, have been conducted to interpret and formulate the wear mechanism of the aircraft brake materials.

Microscopically, the wear particles were examined. The initiation and growth of surface cracks and the oxidation were emphasized in this investigation.

Macroscopically, it has been found for the current copper based brake material sliding against 17-22 AS steel in a caliper brake that the surface temperature (T) raised due to frictional heat is nonlinearly proportional to load (L) applied and slide time (t) with speed at 1750 rpm, i.e.

$$T = P_1 \cdot L^{P_2} \cdot t^{P_3}$$

where P_1, P_2 and P_3 are parameters which could be related to frictional coefficient and other properties of materials associated. The wear ($\triangle W$) of brake materials is then proportional to this temperature with the emphasis of melting point of copper (T*). It yields

$$\triangle W = K \cdot \frac{T}{T^* - T}$$

where K is constant. Essentially, this means that the wear mechanism is a temperature dependency in which the melting of copper matrix plays an important role. A computer program was applied for curve fitting with the experimental data.

Finally, a wear model was proposed and compared with some published wear mechanism concepts.

17. Key Words (Suggested by Author(s)) Wear Particle Surface Temperature Wear Model Scanning Electron Microscopy	18. Distribution Statement Unclassified - unlimited
19. Security Classif. (of this report) Unclassified	20. Security Classif. (of this page) Unclassified	21. No. of Pages 67	22. Price*

NASA-C-168 (Rev. 10-75)

FOREWORD

TABLE OF CONTENTS

SECTION 1

SUMMARY

An initial investigation of both worn surfaces of friction pads and steel rotors which are being applied in current aircraft brakes has been carried out by employing electron microprobe and x-ray diffraction analysis. It consists of the topographical study and the analysis of chemical element distribution.

Based upon this initial examination, two approaches, microscopic and macroscopic, have been conducted to interpret and formulate the wear mechanism of the aircraft brake materials.

Microscopically, the wear particles were examined. The initiation and growth of surface cracks and the oxidation were emphasized in this investigation.

Macroscopically, it has been found for the current copper based brake material sliding against 17-22 AS steel in a caliper brake that the surface temperature (T) raised due to frictional heat is nonlinearly proportional to load (L) applied and slide time (t) with speed at 1750 rpm, i.e.

$$T = P_1 \cdot L^{P_2} \cdot t^{P_3}$$

where P_1, P_2 and P_3 are parameters which could be related to frictional coefficient and other properties of materials associated. The wear (ΔW) of brake materials is then proportional to this temperature with the emphasis of melting point of copper (T^*). It yields

$$\Delta W = K \cdot \frac{T}{T^* - T}$$

where K is constant. Essentially, this means that the wear mechanism is a temperature dependency in which the melting of copper matrix plays an important role. A computer program was applied for curve fitting with the experimental data.

Finally, a wear model was proposed and compared with some published wear mechanism concepts.

SECTION 2

INTRODUCTION

From the safety aspect, two frictional properties of brake materials are important. First, in order to avoid friction induced vibrations known as "squeal", the friction should not vary with velocity. Second, the friction should not decrease with temperature, thus reducing the tendency of brakes to fade.

Knowledge providing insight into the braking process will make the development work of brake materials easier. Recently, several wear studies which are plausible and promising have been established to interpret and predict the wear behavior under certain circumstances. For example, Bill and Wisander's "Surface Recrystallization Theory" (Refs.1 and 2) applicable to a soft metal (Cu) sliding against a hard metal (440 C steel) in liquid methane proposed a wear model based on the extensive plastic deformation in the surface recrystallized layer. The thickness of this layer is proportional to the sliding velocity as well as the shear yield stress. Suh (Refs.3 and 4) described the "delamination" theory of wear by observing the sliding of metals at low speeds only. The theory is valid when there is no significant temperature rise at the surfaces. This dislocation mechanism of wear emphasizes on that the subsurface deformation which induces the coalescence of voids and cracks causes eventually the formation of thin wear sheets. In Reference 5, a deformation/smoothening process of wear particle formation was investigated for lubricated bronze sliding against steel under a light load. Also, the Ferrographic techniques have been developed by Westcott (Refs.6 and 7) to analyze and classify the wear particles mainly obtained from the oil samples of bearing or transmission systems. However, there is no definite theory published involving both the physical and chemical problems in brake mechanics. Accordingly, research efforts in the Tribology Laboratory of RPI have been initiated in this specific field under the project "Mechanics of High-Energy Brake Systems." In this project an initial investigation of the current brake materials was reported, (Ref.8) some new suggested brake materials were presented, (Ref.9) and evaluated by using a full-scale testing (Ref.10). The frictional studies of nickel-based materials

have been underway to improve the friction-velocity behavior of these newly developed materials (Ref.11). Also the fundamental studies on wear mechanism have been undertaken along with the material development and evaluation. The following report is a summary of these wear studies compared with other published wear mechanism concepts.

SECTION 3

INITIAL INVESTIGATION OF THE WORN SURFACES OF CURRENT
AIRCRAFT BRAKE MATERIAL AND ROTOR STEEL

Electron Microprobe Analysis

An investigation of the surfaces of a used brake pad (with over about
50% spallation) and an unused pad of the same material employed in current
aircraft brakes has been carried out. This investigation consists of a
topographical study in the scanning electron micrographs and the analysis
of chemical element distribution detected by following three different
methods of electron microprobe analytical approach (Ref.12). The first,
electron composition imaging, utilizes solid-state paired electron detectors
to provide a magnified image of varying contrast of the specimen surface,
wherein areas rich in high-atomic-number elements appear bright and those
rich in low-atomic-number elements appear dark. This map also contains
some topographic information which aids in the interpretation. The second,
characteristic X-ray emission imaging, produces a magnified image of white
dots on a black ground, wherein the density of white dots is an indication
of the distribution in the specimen surface of the particular element selected
for investigation. The third, characteristic X-ray line scan, yields a CRT
trace of varying amplitudes as the electron beam is caused to traverse a
straight line across some selected path in the magnified electron composition
image of the specimen surface. The beam path and the X-ray signal amplitude
variations, are superposed photographically on the electron composition
image to facilitate correlation of element concentration variations with
recognizable microscopic features of the specimen surface. The third method
is the most sensitive method, and it was used only for mapping a chemical
element present in low concentration (e.g., chromium) or one which produces
a relatively weak X-ray signal (e.g., carbon).

The scanning electron micrographs of the surface of a worn pad which
was obtained from actual brake assembly in an area where some spalling
occurred, are shown in Figure 1. The smooth regions appear severely smeared,
whereas the spalled regions are rough cavities.
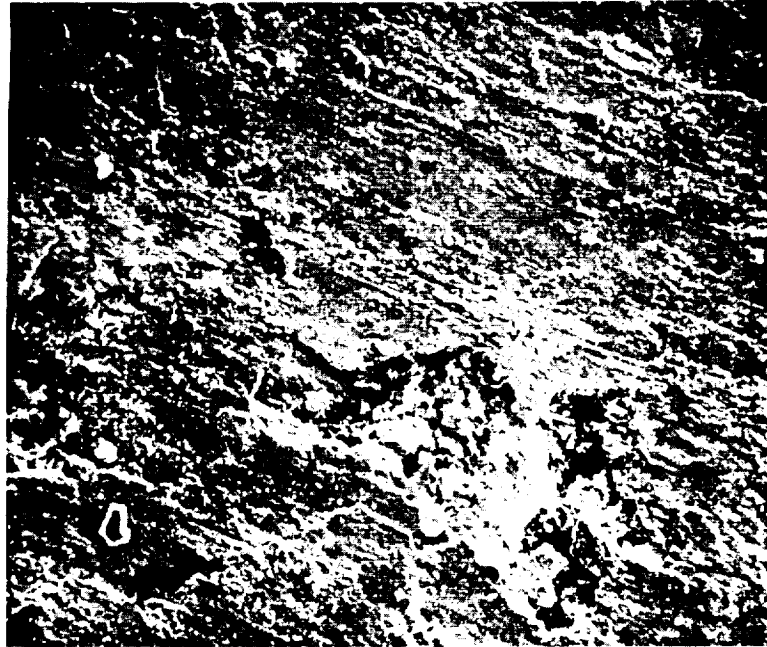
A.   100X
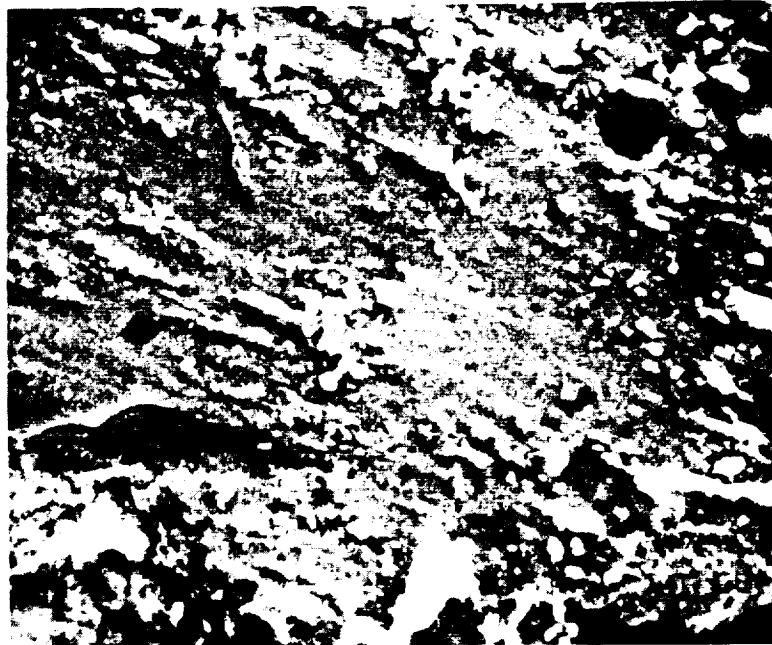
B.   1,000X

FIGURE 1. Scanning Electron Micrographs of Surface
of Smooth Region in Brake Pad

In Figure 2, the smooth area (upper half of micrographs) exhibits high concentrations of copper and iron, together with small amounts of chromium and nickel. In the spall depression (lower half), aluminum appears. In the spall depression (Figure 3), the region rich in copper contains only a small amount of iron and no chromium; the aluminum and carbon are separately situated in other microscopic regions.

Similar analyses of an unused pad specimen (area A) showed the copper and iron to be essentially located in separate regions (Figures 4B and C), with some nickel associated with the iron (Figure 4D); no chromium was detected. The aluminum occurs in other discrete regions (Figure 4E). In another area (B) of this specimen (Figure 5A), the carbon (Figure 5B), copper (Figure 5D), iron (Figure 5E) and aluminum (Figure 5G), all are situated in separate microscopic regions, the small amount of nickel appears to be associated with both the copper and the iron (Figure 5F). No chromium was detected.

Accordingly, the composite material of the pads contains (by volume %) about 31% Cu, 22% mullite (3 Al_2O_3 · $2SiO_2$), 32% graphite and 15% friction modifiers (iron, lead, tin, etc.) (Ref.13). The mating material of the rotor is 17-22 AS steel (0.30 C, 0.50 Mn, 0.25 Si, 0.040 P, 1.0 Cr, 0.50 Mo, and 0.25 V). This electron microprobe analysis has detected copper, iron, carbon (graphite), aluminum (Al_2O_3), and nickel in the new pad. Neither lead nor tin could be detected. In the surfaces of the worn pads, these same elements (Cu, Fe, C, Al and Ni) were found, plus chromium. This means that the iron of the unused pad material does not contain chromium, but the iron (containing chromium) of the mating steel rotor surface transferred to the worn pad during brake performance. In other words, the material transfer detected by this technique is a significant factor in later determination of the wear mechanism for aircraft brake materials.

A. Electron Composition Image

B. Copper X-Ray Image

C. Iron X-Ray Image

D. Chromium X-Ray Image

FIGURE 2. Electron Microprobe Analyzer Images of Surface of Brake
Pad   Field Spans Smooth Plateau (Upper-Half)
and Spall Depression (Lower-Half)
100X

7.
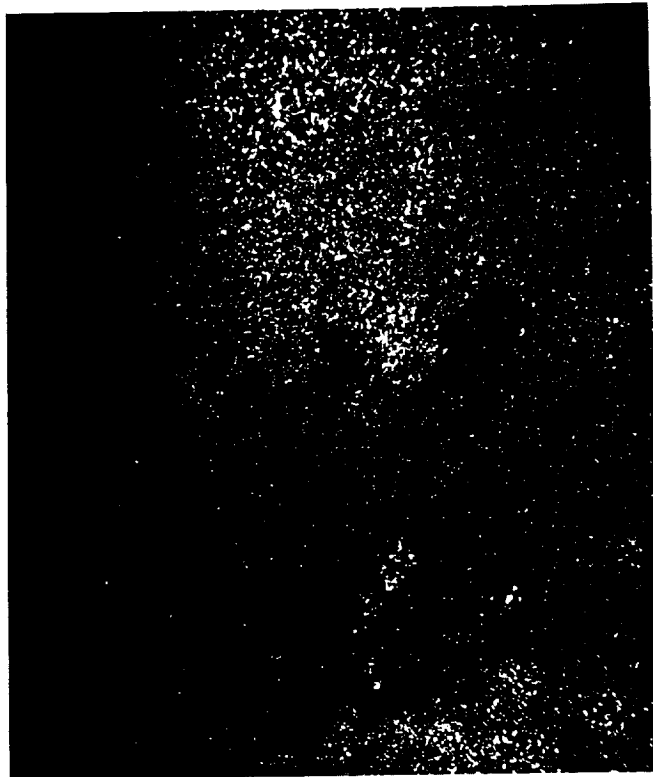
E. Nickel X-Ray Image No. 1104
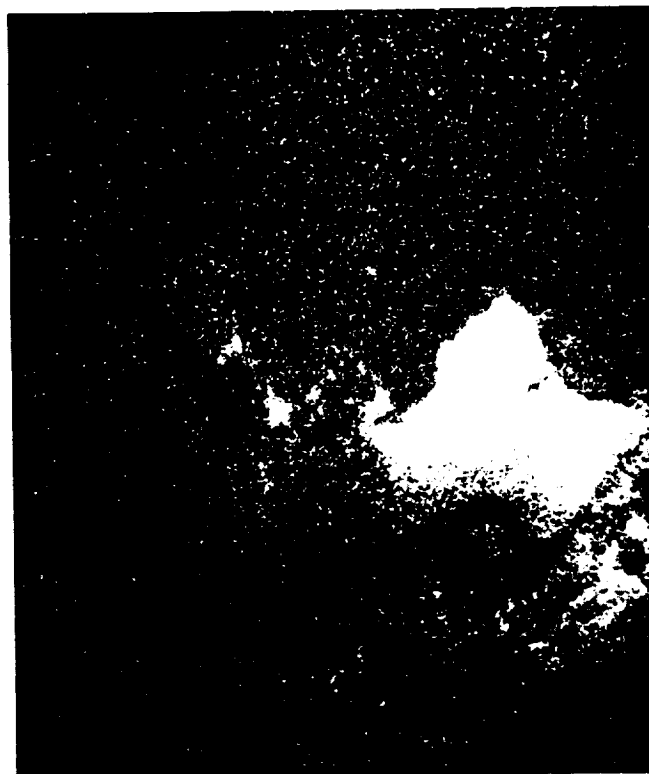
F. Aluminum X-Ray Image

FIGURE 2 (cont'd). Electron Microprobe Analyzer
Images of Surface of Brake Pad
Field Spans Smooth Plateau (Upper-Half)
and Spall Depression (Lower-Half)
100X
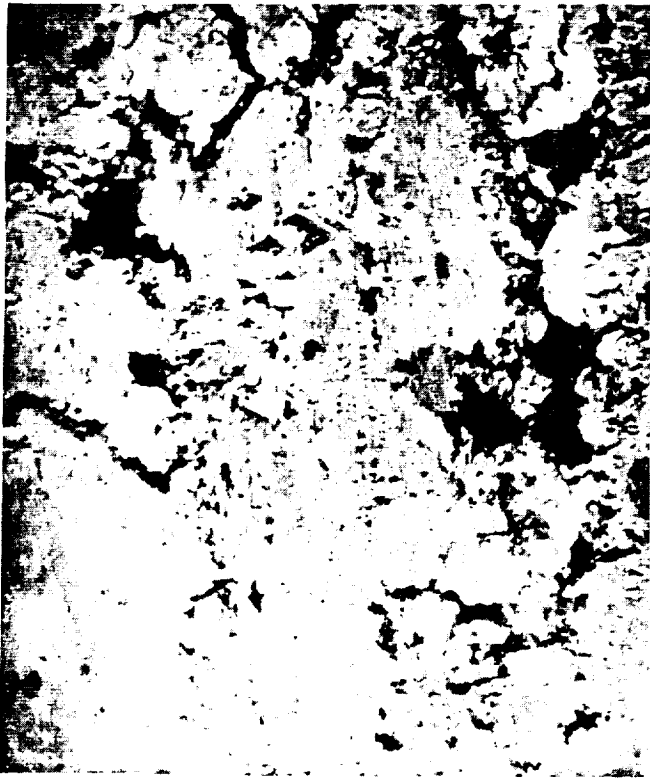
A.   Electron Composition Image   B.   Copper X-Ray Image
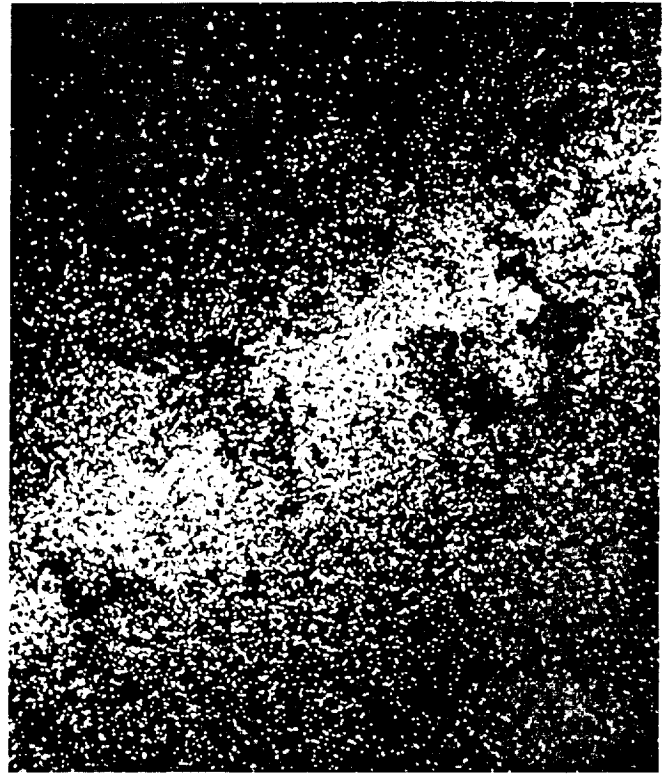
C.   Iron X-Ray Image   D.   Aluminum X-Ray Image

FIGURE 3.   Electron Microprobe Analyzer Images
of Surface of Brake Pad
Spall Depression Region
100X

E. Carbon X-Ray Image
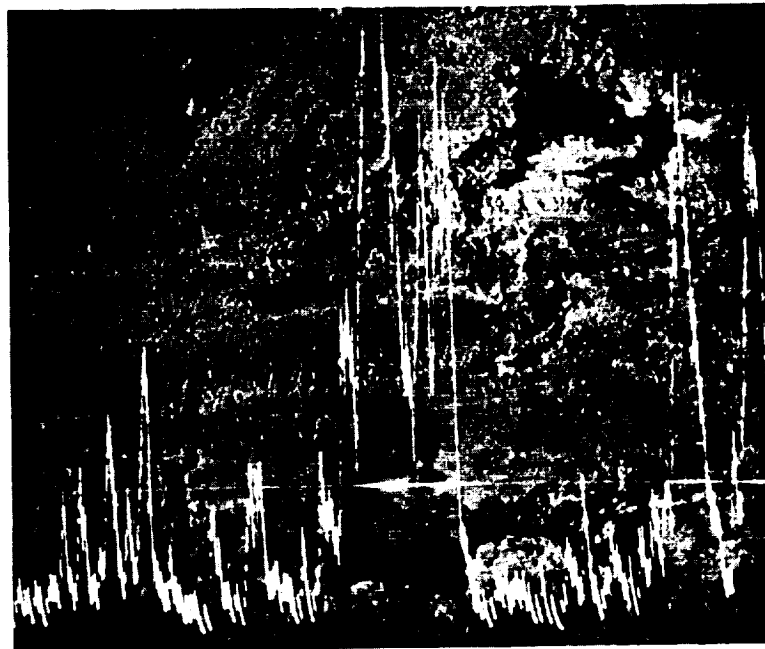
F. Carbon X-Ray Line-Scan Superposed
    on Electron Composition Image

FIGURE 3 (cont'd). Electron Microprobe Analyzer Images
        of Surface of Brake Pad   Spall
        Depression Region. Micrographs Rotated 90°
        Clockwise with Respect to Figure 3 A-D.
                100X

A. Electron Composition Image
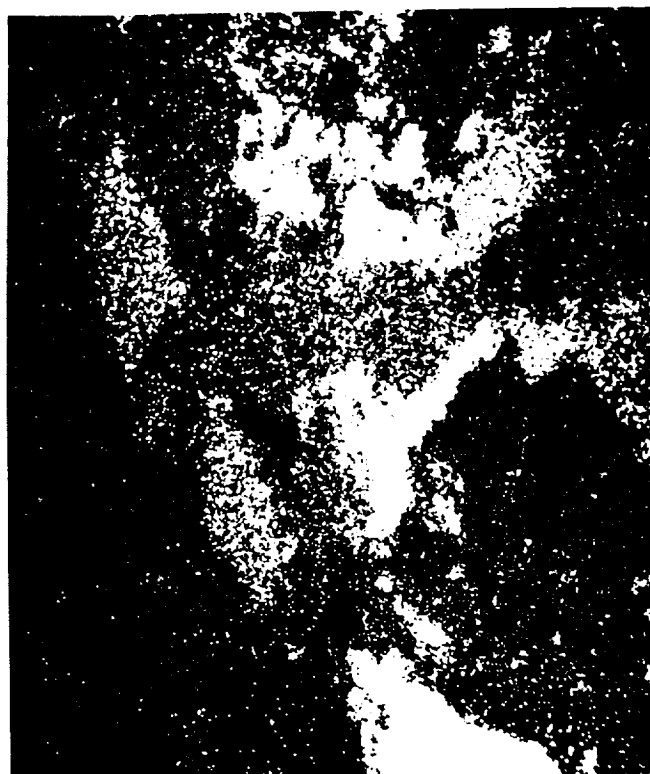
B. Copper X-Ray Image

C. Iron X-Ray Image

D. Nickel X-Ray Image

FIGURE 4. Electron Microprobe Analyzer Images of Surface
of Unused Brake Pad - Area A
100X
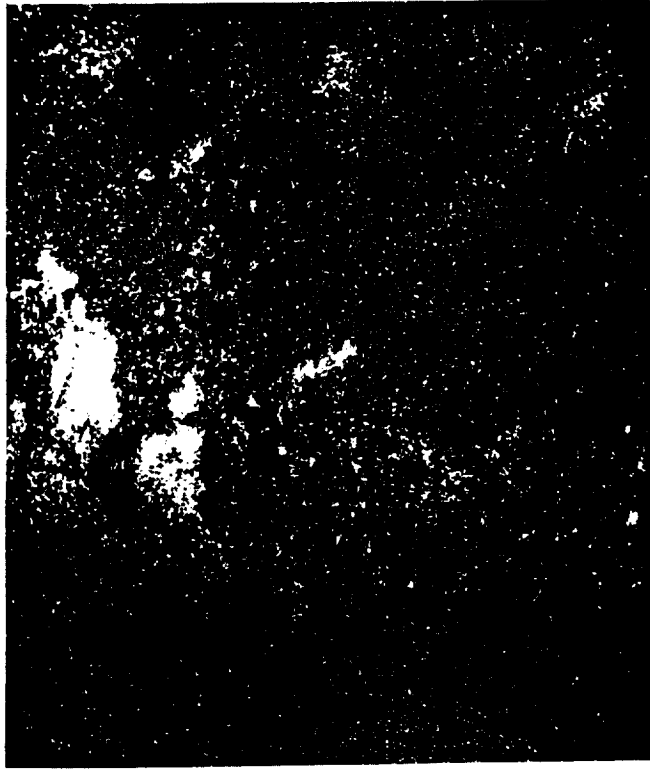
E.   100X

FIGURE 4.(cont'd). Electron Microprobe Analyzer Aluminum
            X-Ray Image of Surface of Unused Brake Pad--Area A

A. Electron Composition Image

B. Carbon X-Ray Image

FIGURE 5 Electron Microprobe Analyzer Images of Surface
of Unused Brake Pad - Area B
100X

13.

C. Electron Composition Image

D. Copper X-Ray Image

E. Iron X-Ray Image

F. Nickel X-Ray Image

FIGURE 5 (cont'd). Electron Microprobe Analyzer Images
of Surface of Unused Brake Pad - Area B
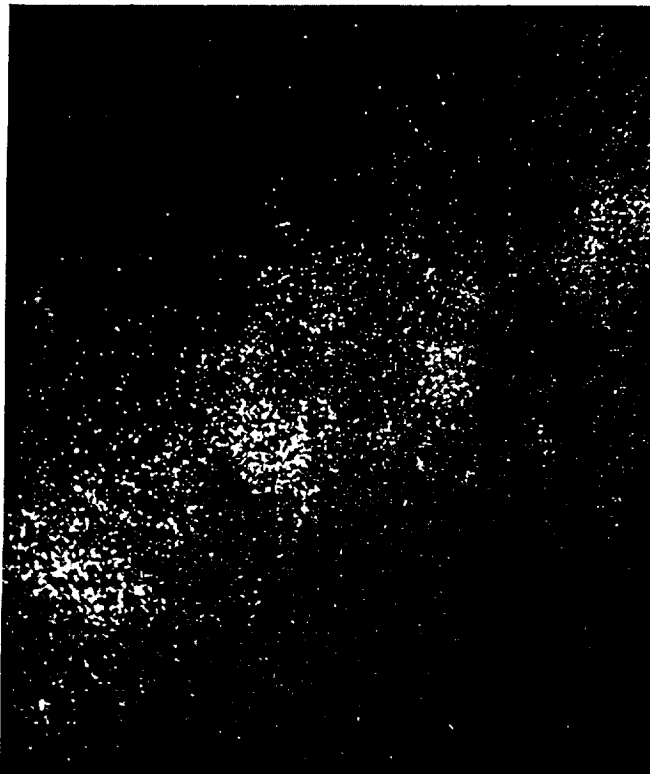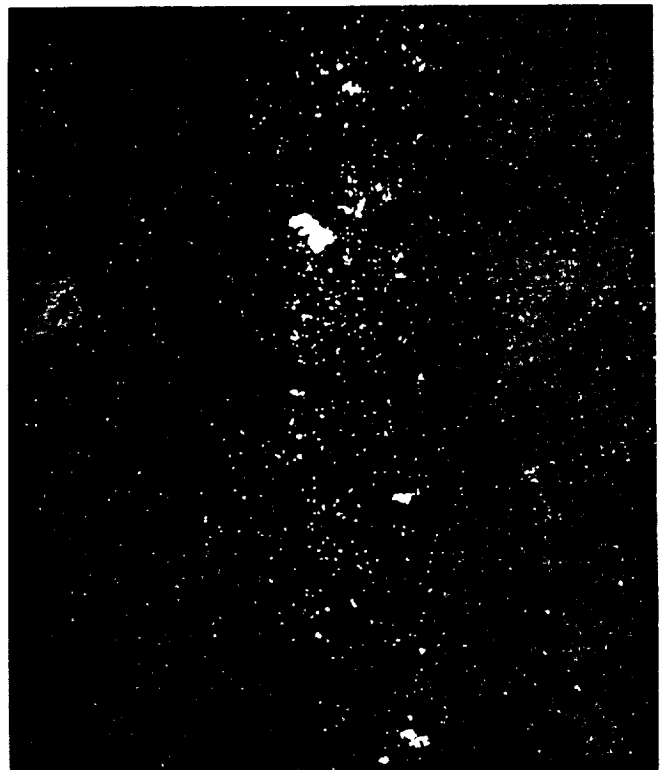500X

14.

G. Aluminum X-Ray Image

FIGURE 5 (cont'd). Electron Microprobe Analyzer Images
of Surface of Unused Brake Pad - Area B
500X

X-Ray Diffraction Analysis
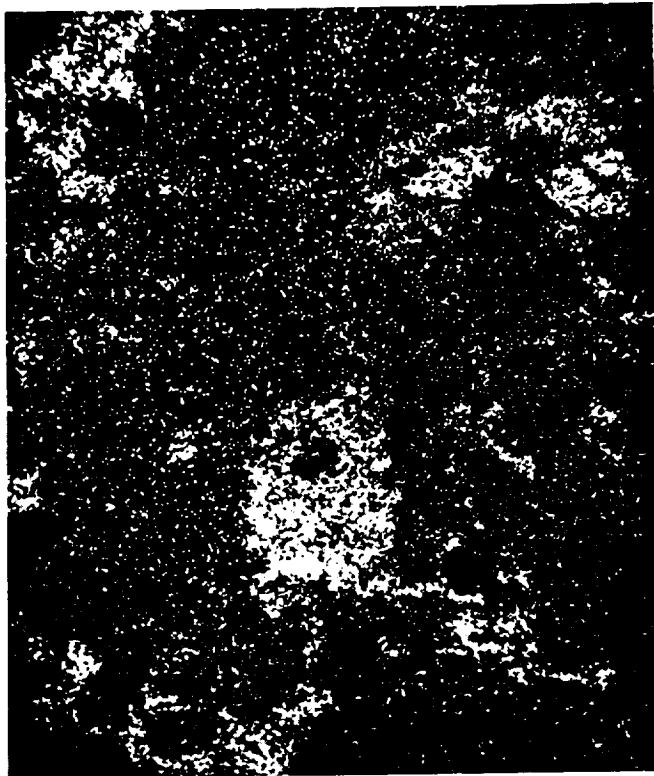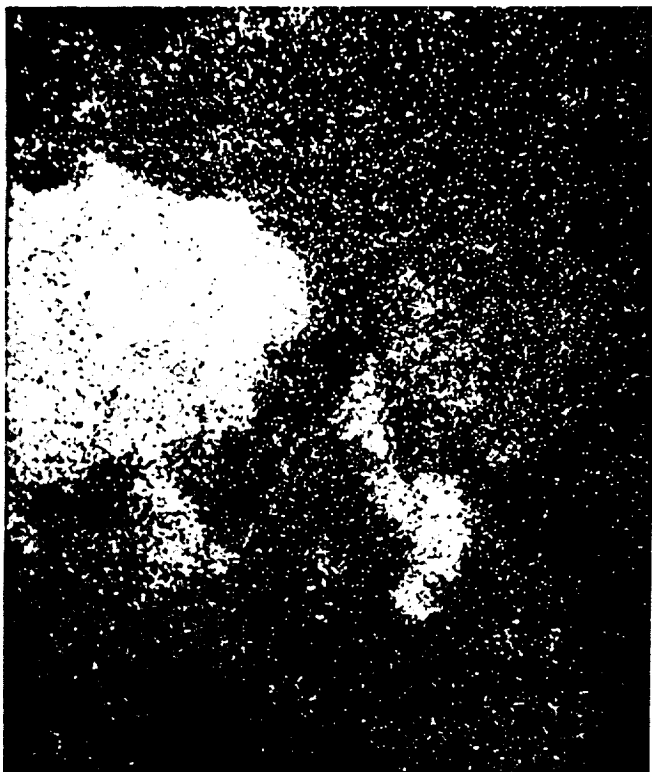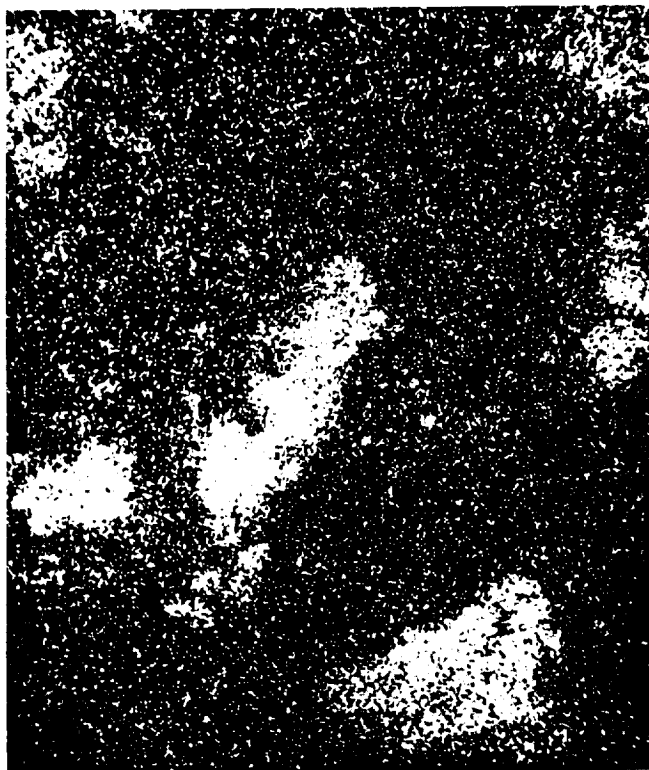
The X-ray diffraction technique (Ref.14) has been employed for the surface studies of current copper-based brake materials. The diffraction pattern showed cuprous oxide (Cu_2O), wüstite (FeO), hematite (α-Fe_2O_3 and γ-Fe_2O_3) and magnetite (Fe_3O_4) in the sliding surface of a used pad. Cuprous oxide (Cu_2O) gave the highest concentration in the sliding surface. No notable amount of iron was found. Iron oxides are found as a consequence of the material transfer from the steel rotor to the brake pad during rubbing against each other.

Also this X-ray diffraction method was used to observe the surface which was obtained after the pad material had been sanded down 3.8×10^{-4} meter (0.004") deeper. It was found that all of the oxides mentioned before still exist, however their concentrations decrease except for the case of wüstite (FeO).

A summary of the results is shown in Figure 6. The X-ray intensity of components of three surfaces was plotted versus the surface depth from the sliding surface. A sharp decrease of cuprous oxide (Cu_2O) with a correspondingly tremendous increase of copper is seen along the depth from the sliding surface. It is reasonable that heavy oxidation took place on the sliding surface due to high interface temperature. The oxidation is reduced along the temperature gradient inwards.

At the sliding surface, the hematites (α-Fe_2O_3 and γ-Fe_2O_3) yield the highest values of intensity among the iron oxides, magnetite (Fe_3O_4) is second. Intensity of the wüstite (FeO) is the lowest. The intensity of the hematites and the magnetite decreases with depth from the sliding surface; but that of the wüstite increases with depth. At a depth of 3.8×10^{-4} meter (0.015") below the sliding surface, Fe_3O_4 yields the highest value of intensity. At the surface level of 1.0×10^{-4} meter (0.004") deeper the intensities are in the order FeO, Fe_3O_4, α-Fe_2O_3 and γ-Fe_2O_3. These results confirm the oxidation mechanism of iron which is in a sequence of O_2/Fe_2O_3/Fe_3O_4/FeO/Fe at the temperatures above about 600°C (Ref. 15). This means that the iron oxides in the pad are balanced and coexist in such a way that the diffusion processes play a dominating role in oxidation during high energy braking (Ref.16).
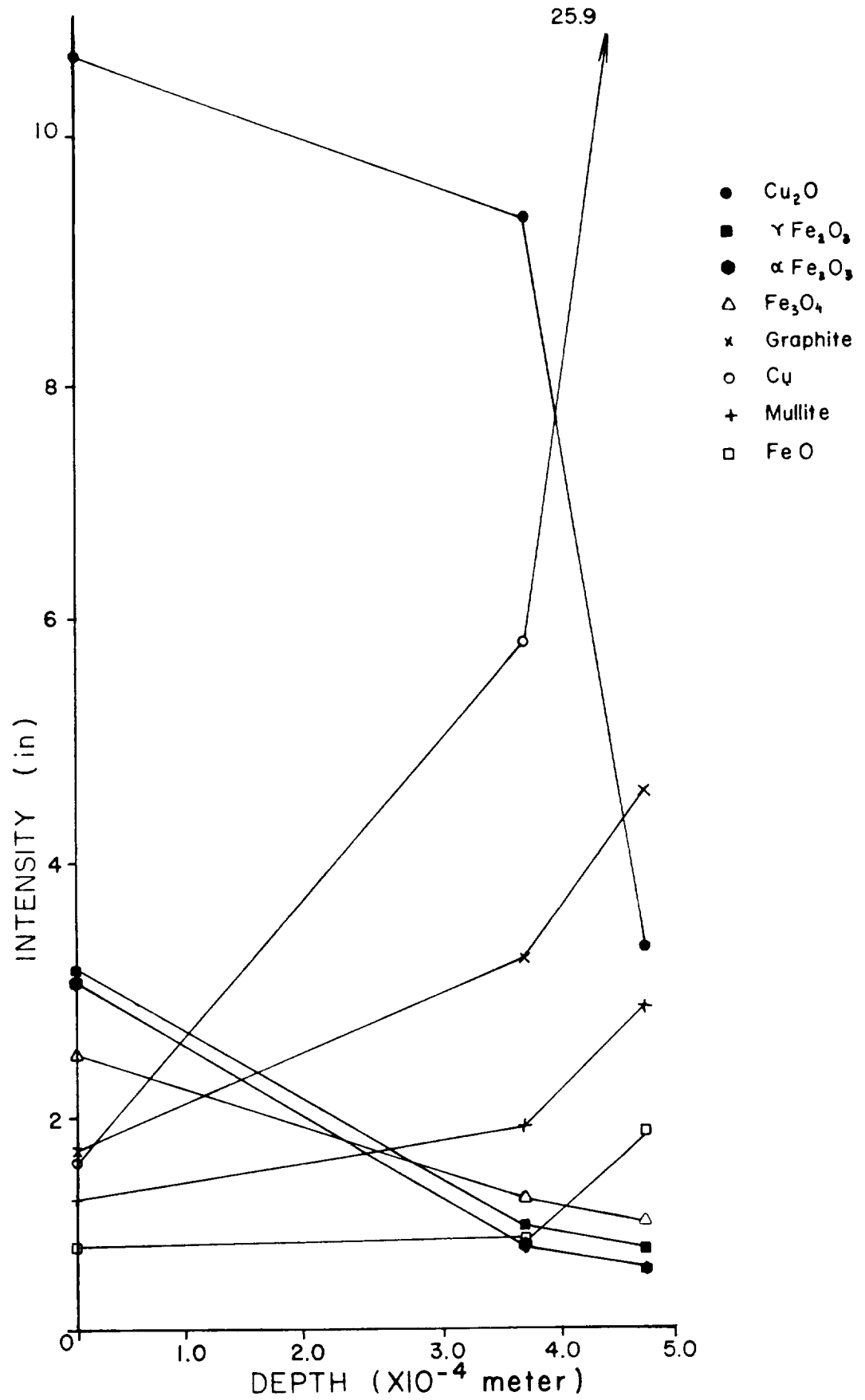
Figure 6   Intensity of Component Versus Depth from the Sliding Surface

A used steel rotor surface was also examined by X-ray diffraction technique. It was found that the major intensity peaks are α-Fe, γ-Fe (austenite), α-Fe$_2$O$_3$, γ-Fe$_2$O$_3$, Fe$_3$O$_4$ and FeO. No notable amount of copper or copper oxide was found.

Although the results are largely what might have been expected, it is significant that no complex oxides were found which could be indicative of the glassy film formation. Secondly, the wear process appears to proceed by the transfer of iron oxide to the pad from which it is removed. It is interesting to note that the actual oxide film thickness as measured on a large number of brake pads is less than 2.54×10^{-5} meter (0.001") (Ref.8). This means that there is considerable in depth oxidation of the bulk material.

SECTION 4

APPARATUS, MATERIALS AND PROCEDURE

Apparatus

For the wear study, two test rigs have been used, which are described as follows:

Rig A

This test facility, shown in Figure 7, was primarily built for the evaluation of brake systems (Ref.10). It consists of a complete brake from a small jet aircraft, a 75-KW AC electric motor and a 175 KW water-cooled eddy current coupling connected in between for varying of velocity from zero to 1750 rpm (Figure 8). The brake has essentially two steel stator plates with annular friction pads face to face to sandwich one disk rotor of 17-22 AS steel (Figure 9).

Rig B

A photograph of the test apparatus is shown as Figure 10, which was built for evaluating new brake materials (Ref.9). It consists of a 30.5 cm-diameter rotating 17-22 AS steel disk (0.79 cm thick) with test buttons (1.9 cm diameter by 1.9 cm long) loaded against opposite faces. The rotating disk is mounted on the drive shaft of a 30-KW AC electric motor. The test specimens are mounted in a holder which is held in a water-cooled jacket. These are mounted in a standard commercial caliper brake. The caliper brake is mounted on a fixed arm (Figure 11).

Each test rig was equipped with a similar set of instruments for monitoring the test information. Essentially, the instrumentation includes the following:

1. A pressure transducer for monitoring air pressure in the brake hydraulic system.
2. A four strain gage torquemeter mounted on the stationary shaft for indicating the frictional torque.
3. A tachometer for monitoring rotational velocity of the disk rotor.
4. A timer for regulating the length of the brake application.

Figure 7   Photograph of Test Apparatus for Brake Material Evaluation (Rig A)

20.

1 – WHEEL HALF

2 – DISC BRAKE

3 – PRESSURE TRANSDUCER

4 – STRAIN GAGE TORQUEMETER

5 – THERMOCOUPLES

6 – TACHOMETER

7 – SOLENOID VALVE

8 – REGULATED COMPRESSED AIR SUPPLY
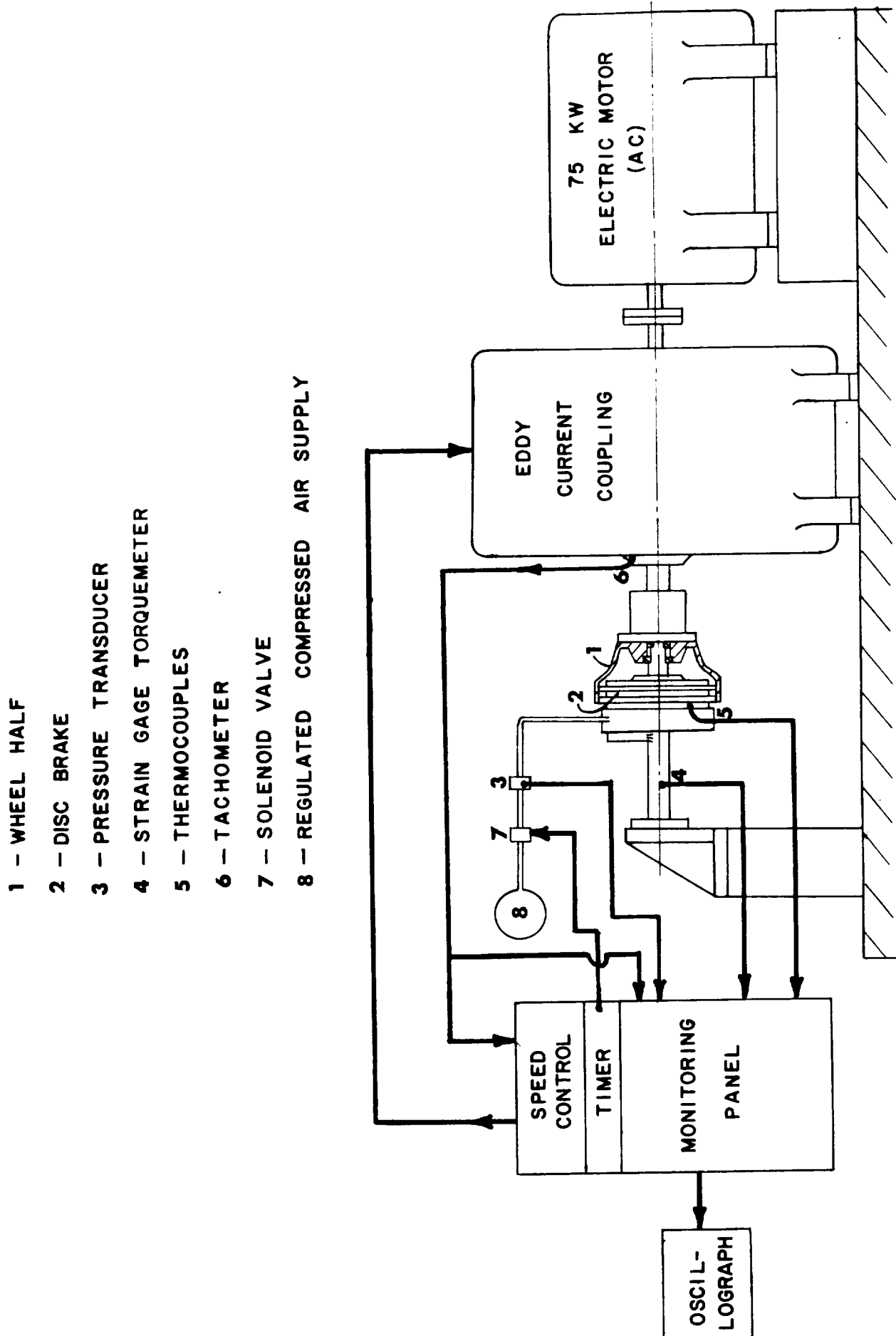
Figure 8   Schematic Diagram of Test Equipment for Brake Material Evaluation
(Rig A)

21.

1.Driving Shaft 7. Back Plate
2.Friction Pad 8.Wheel Half
3.Rotor
4.Stator
5.Stationary Shaft
6.Spacer
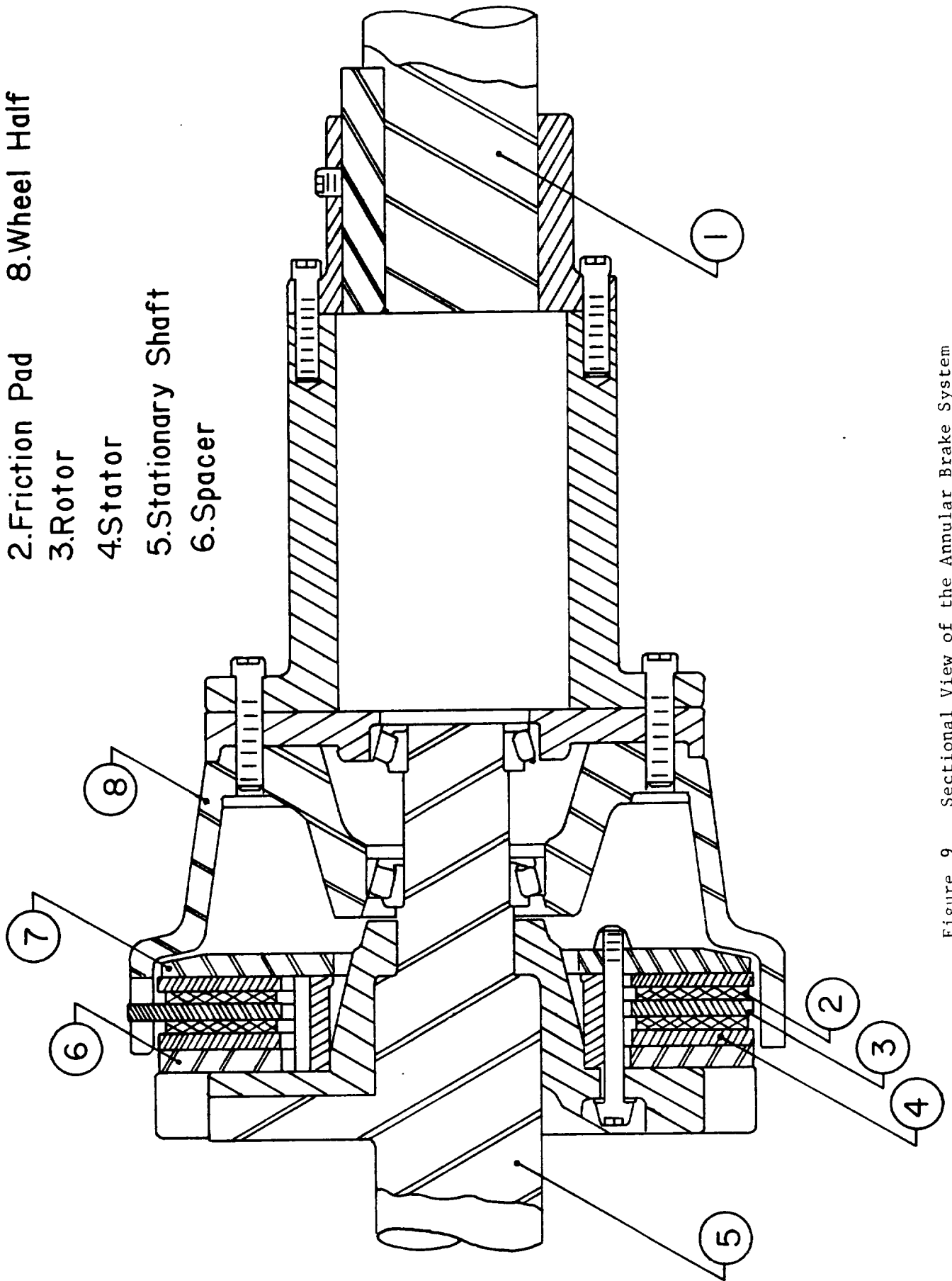
Figure 9   Sectional View of the Annular Brake System

22.
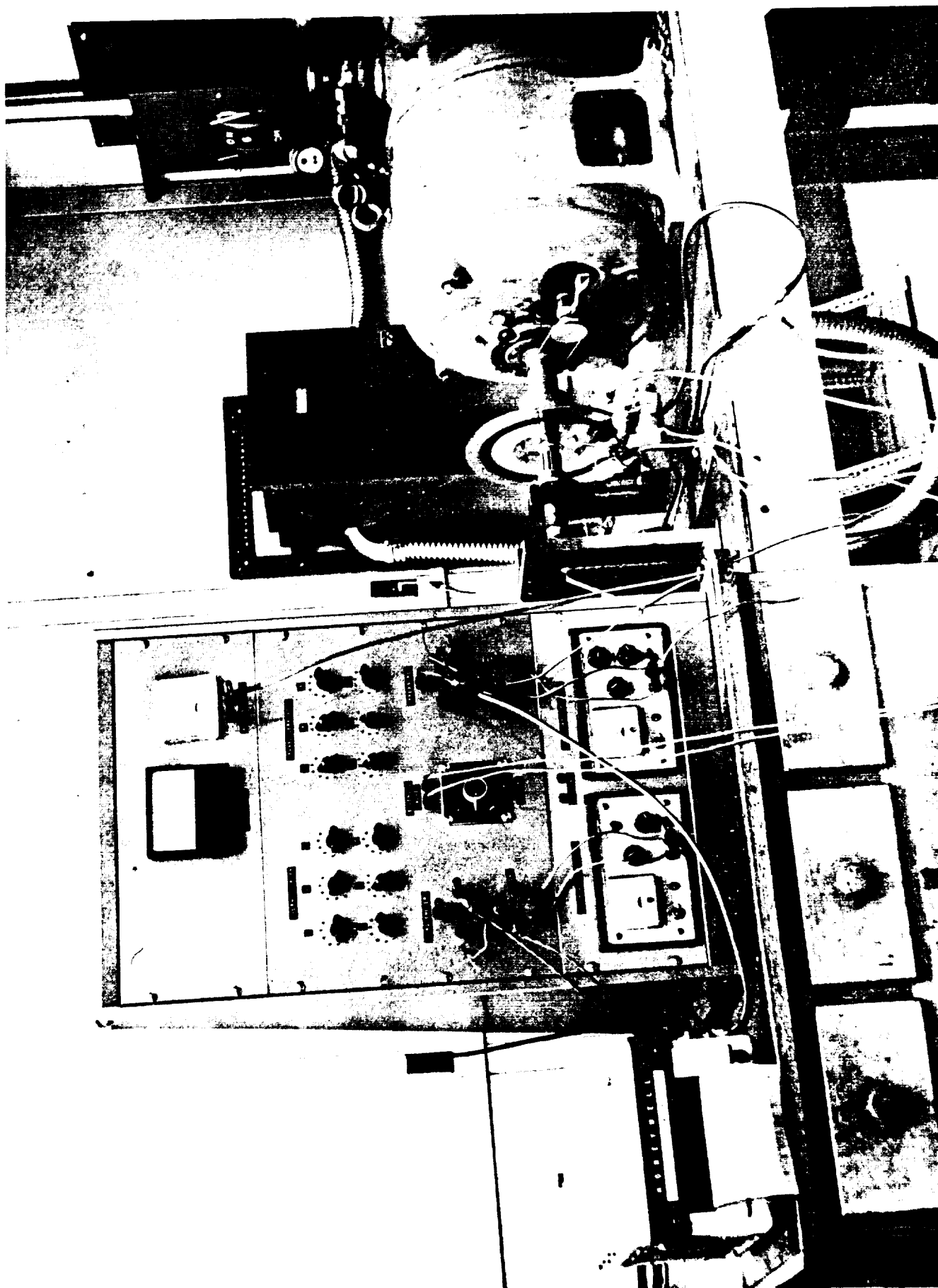
Figure 10 Photograph of Brake Test Apparatus for Material Development (Rig B)

Figure 11   Diagram of Test Apparatus for Brake Development (Rig B)

RECORDER

GALVANOMETER

MOTOR
(30,000 WATT)

COOLING WATER

PRESSURE

SPEED

TEMPERATURE

TORQUE

COMP AIR

CALIPER BRAKE

1. TORQUOMETER
2. THERMOCOUPLES
3. TACHOMETER
4. PRESSURE TRANSDUCERS
5. BUTTON SPECIMENS
6. DISK (17-22 AS STEEL)

ω = 183 RAD/SEC

V = 22 m/SEC

305 mm D

19 mm D

120 mm

24.

5. Chromel-alumel thermocouples, located in the stationary specimens within 1.59 mm from the sliding surface, for measuring near-surface temperatures.

All data read-out was recorded simultaneously on a 12-channel oscillograph so that direct comparison of changes could be made during brake operation. All devices were carefully calibrated before the test program and the calibrations were checked occasionally during the investigation.

Materials and Procedure

Two different test procedures were followed to acquire information relative to the wear behavior of brake materials. They are as follows:

1. General Survey. Test rig A was used, and various materials slid against 17-22 AS steel. These materials were copper base, nickel base, Mo-Tribaloy, and carbon. Their chemical compositions are listed in Table 1. A variety of test conditions were used, with increasing severity, until a temperature of 730°C was reached. Wear particles were collected and an examination of the surface was made at each condition. The main purpose of this survey was to find an early criterion of surface fracture and wear.

2. Effect of Variables. In this study, only the current copper-based brake material was tested sliding against 17-22 AS steel under a series of test conditions which are the combinations of two test variables, load (L) and slide time (t), while maintaining the velocity (V) constant. The effects of the variables on wear and surface conditions are studied in order to formulate a wear theory for the aircraft brake systems. Also the criterion of the surface fracture wear will be analyzed in detail in this investigation. Rig B was used. The velocity was held constant at maximum value of 1750 rpm for the steel rotor disk. The surface conditions of the brake material and wear particles were examined with the scanning electron microscope and energy probe. The results will be discussed in the next section.

TABLE 1

CHEMICAL COMPOSITION OF FRICTION PADS

Function	Copper Based	Nickel Based	Mo/LPA 100	Carbon
Base Matrix	Cu (31.0%)	Ni (47.6%)	Mo (50.0%)	C (100%)
Lubricant	Graphite (32.0%)	Graphite (27.5%) (Flake)	-	-
Abrasive	Mullite (22.0%)	Al_2O_3 (19.8%)	-	-
Friction Modifiers	? (15.0%)	$PbWO_4$ (5.0%)	LPA100 (50.0%)	-

SECTION 5

RESULTS AND DISCUSSION

General Survey of Wear Behavior

In order to gain insight into the wear behavior, wear particles were captured under a variety of conditions and examined. Rig A was applied in this phase. The results are described in the following sections.

1) Current Copper-Based Brake Material

Although tests were run and wear particles collected under a large variety of conditions it was found by careful examination that there was very little difference in the nature of the wear debris or the size. In general the wear consisted of flat plates of average size about 3.3×10^{-4} meter $\times 2.2 \times 10^{-4} \times 0.3 \times 10^{-4}$.

Four such sheet-like particles are shown in Figure 12. Three micrographs, "a", "b" and "c" show the sliding surface sides, picture "d" gives a view of the fracture surface in which lots of cracks are seen. Figures 13a and b show the irregularity of the fracture surfaces at higher magnifications. The small particles connected on the surface are thought to be oxides and the hole to be the site where a large particle (may be abrasive) was imbedded and removed.

The removal of the wear plateletts is shown in Figures 13c and d. It is felt that subsurface cracking underneath the interface has taken place before the sheet-like particle can leave. Lots of oxides stay on the substrate where debris was detached (see left of Figure 13c). Also the sliding tracks are seen on the heavily oxidized substrate which locates left as shown in Figure 13d.

In Figure 14, a wear particle is shown in three different views labeled "a", "b" and "c", respectively. The size is about 18×10^{-4} meter $\times 7 \times 10^{-4} \times 2.5 \times 10^{-4}$. This sheet-like particle has a facet with frictional tracks which is shown at higher magnifications in picture "d" (200 $\times$) and "e" (2000 $\times$). It appears that the tracks are covered by a smooth and thin film which resulted from high frictional heating. The rest surrounding the particle is the failure surface of irregular geometry (see Figure 14b).
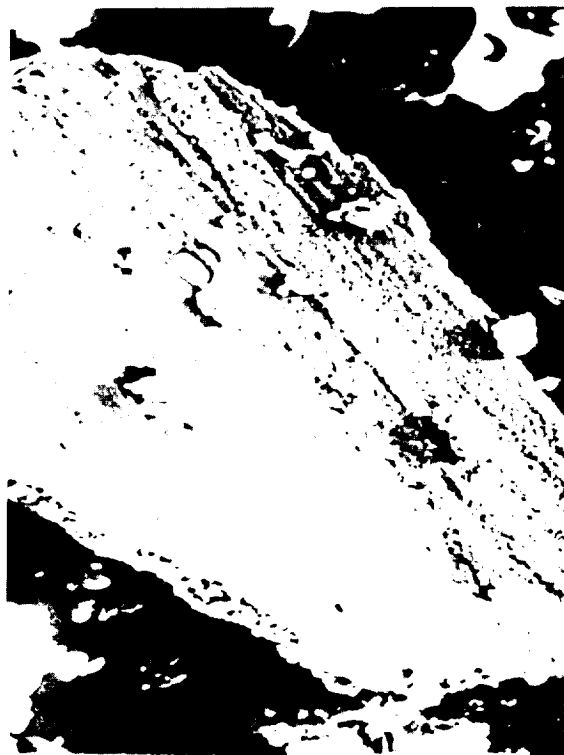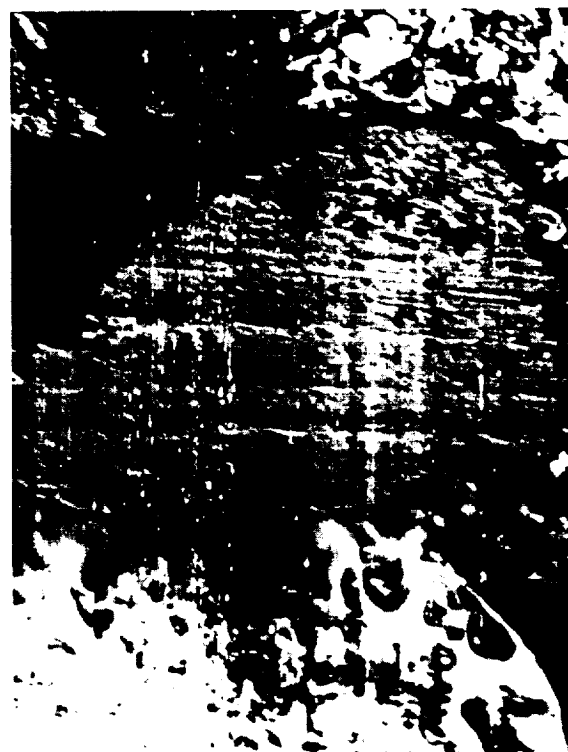
Figure 12 SEM Photographs Showing Four Sheet-Like Particles Collected from the Tests of Cu-Based Brake Material Sliding Against Steel

28.

× 100

c

× 200

d

× 200

a

× 100

b

Figure 13   SEM Photographs Showing Four Different Surface Conditions of Wear Particles Collected from the Tests of Cu-Based Brake Materials Sliding Against Steel.

29.
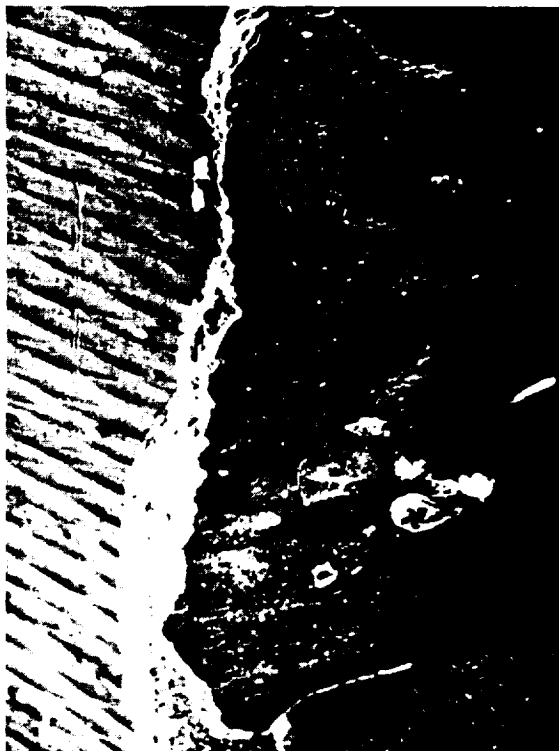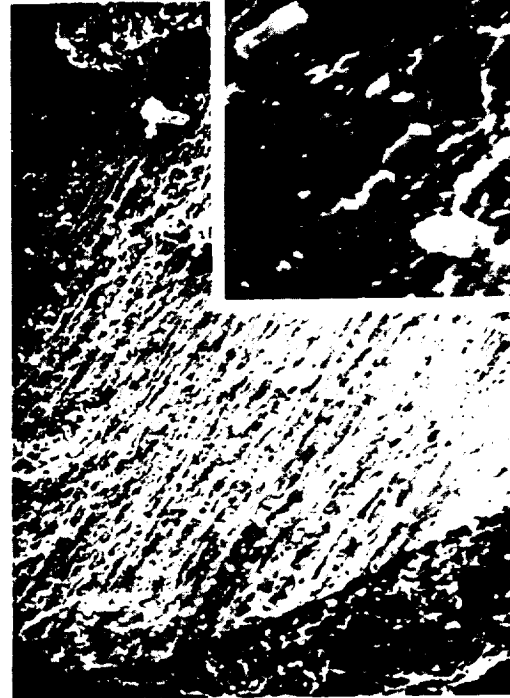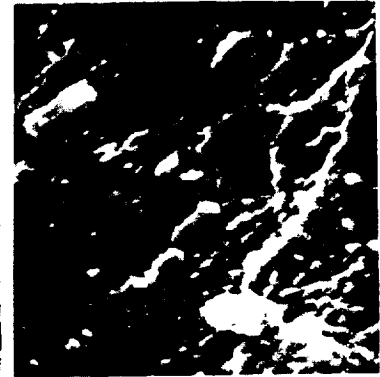
Figure 14 SEM Photographs Showing Three Views and Sliding Surfaces of a Wear Particle of Cu-Based Brake Material Sliding Against Steel

× 50

× 50

× 50

× 200

× 2000

a

b

c

d

e

Two things are noticeable here. First, the side curve of the sliding surface is slightly convex. It is felt that this bending is due to stress relief. Second, two large particles associated with the subsurface cracks which are parallel to and below the sliding surface are found in the left of the picture.

Appreciable further examinations were made to determine where the cracks initiate and how they grow. A typical crack in the particle shown in the last figure can be traced by starting at the sliding surface. Figure 15a indicates the site where the crack joins other cracks in front of a large elliptical particle. The crack extends along the direction of sliding (as shown in Figure 15b), continuing to the edge of the sliding surface (see Figure 16), then extending vertically from the sliding surface (see Figure 17a). The higher magnification of 2000 was applied to examine the crack carefully as shown in Figures 17b and c. It is seen that the upper portion near sliding surface shows the clearer crack due to the more densification of material by loading compact. It becomes less clearly defined at lower depths with lots of loose material on the two sides.

Based upon the observation above, the attention is focused on two pictures shown in Figures 18a and b to interpret the initiation of cracks. The crack starts around a site of hard and relatively large particle embedded in the surface. Weakness resulted around this particle probably from the differences of material properties between particle and its surroundings. For example, the difference in modulus or thermal expansion will result in the material separation around the particle especially at higher temperatures.

In general, there are three planes along which the cracks can grow. They may grow along the sliding direction as mentioned in Figures 15, 16 and 17. This kind of crack is also indicated in Figure 18a as "Crack 1." It grows mainly due to the "Barber Effect" (Ref.17) which is a problem of thermoelastic and thermoplastic instabilities in the sliding. This effect is due to the uneven loading distribution which results from the irregularity of contact surface. The more concentrated loading in the discrete areas will cause more thermal distortion on the sliding surface layer because of the nonuniform heat generation by friction. All these mechanical and thermal disturbances will, no doubt, result in the cracks on the sliding surface
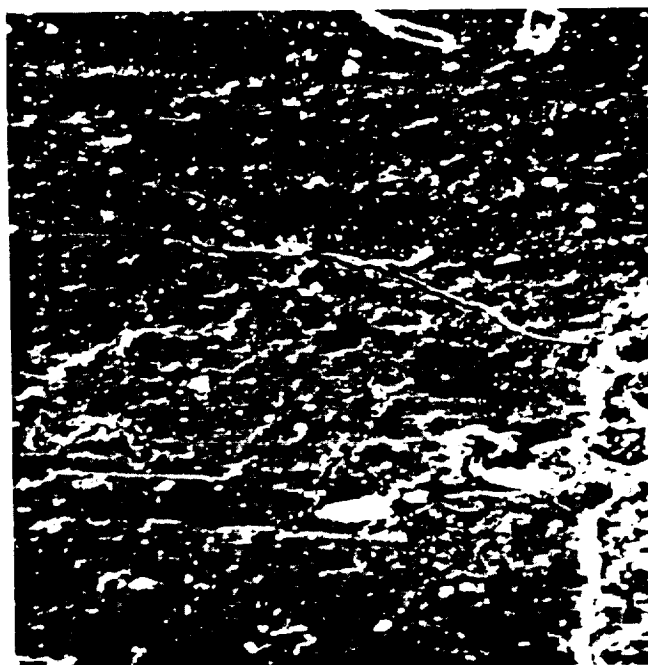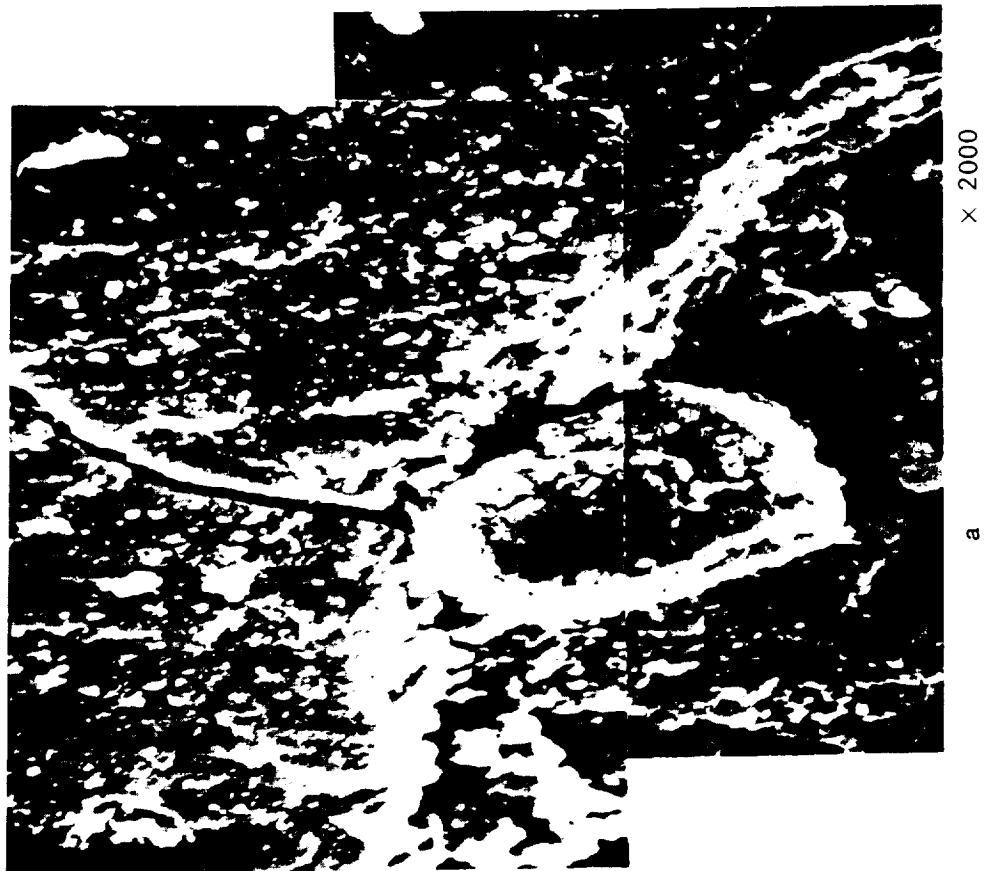
Figure 15   SEM photographs Showing the Initiation and Growth on the Sliding Surface of Particle Shown in Figure 14

× 2000   a

× 500   b

a   × 500
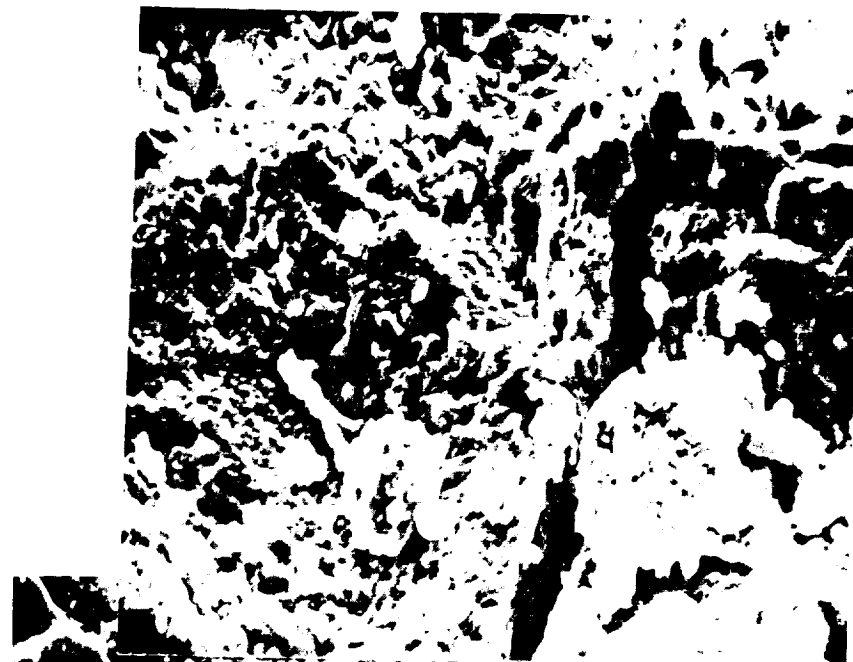
b   × 2000

Figure 16 SEM Photographs Showing the Crack in the Sliding Surface
of the Same Particle in Figure 14

33.

× 2000

b

× 500

a
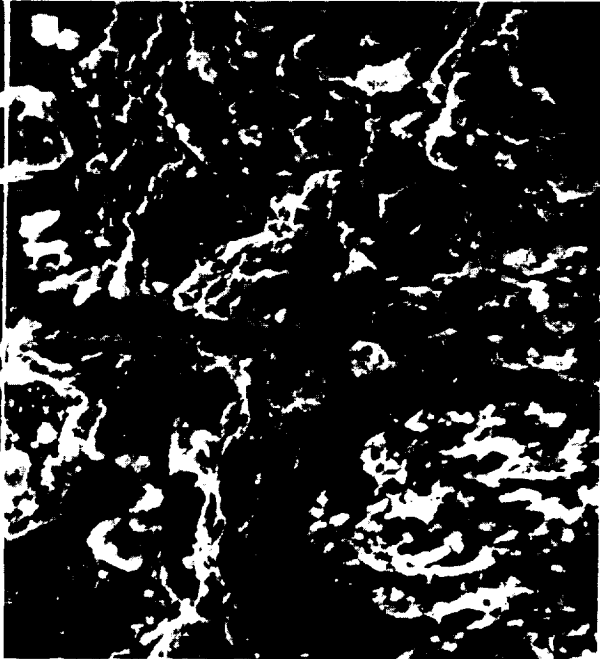
Figure 17 SEM Photographs Showing the Crack on a Lateral Side of the Same Wear Particle in Figure 14

Figure 17 - cont'd.

35.
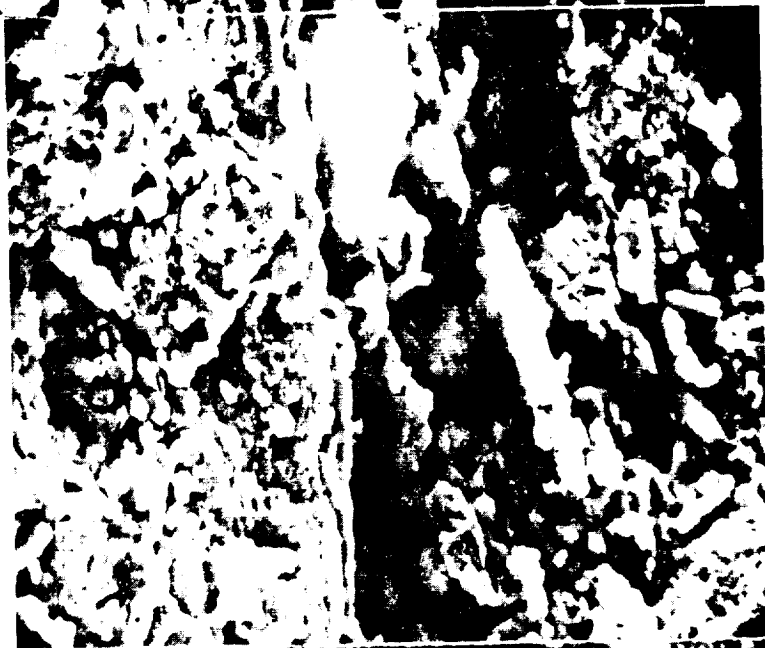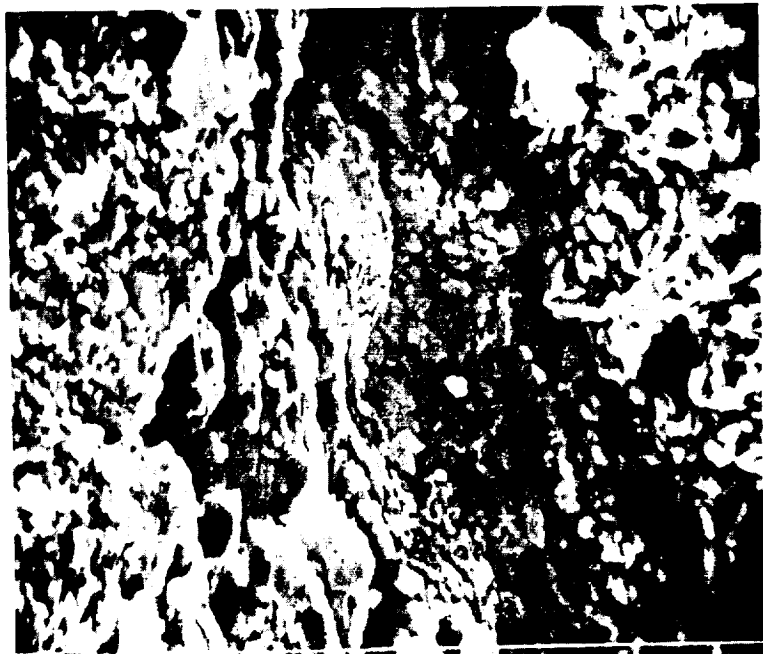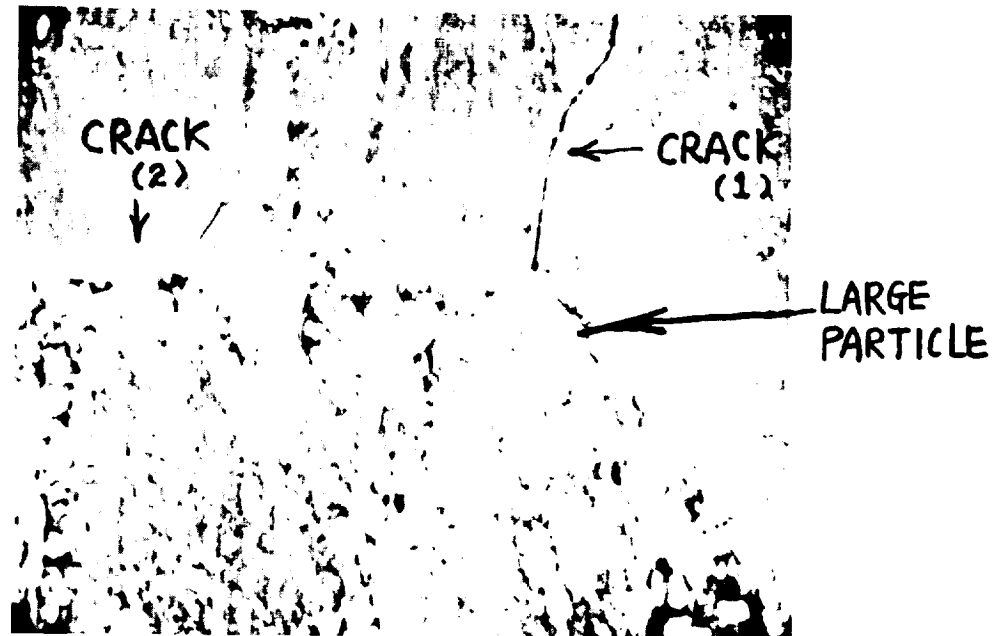
(a)   × 1000
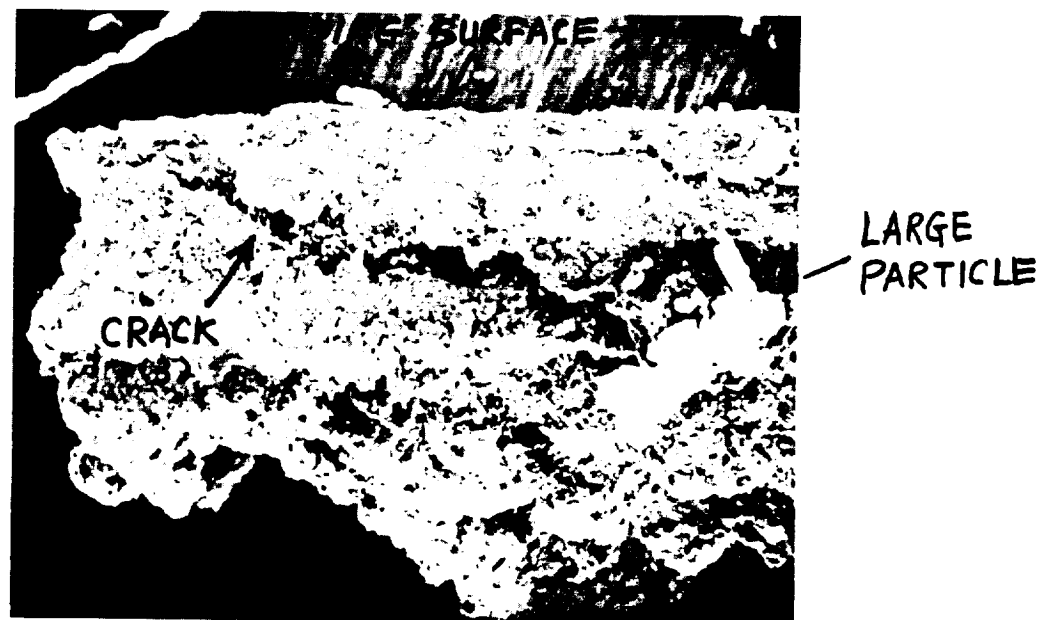
(b)   × 200

Figure 18   Two SEM Photographs Showing the Initiation and Propagation
of Cracks in a Wear Particle of Cu-Based Brake Material
Sliding Against Steel.

layer. Also the frictional force will accelerate the growth of cracks across the sliding direction, which is labeled as "Crack 2" in Figure 18a. The third one (see Figure 18b, "Crack 3") grows parallel to and below the sliding surface to form a "subsurface crack". This results from material fatigue during the sliding; the oxidation accelerates this separation.

2) Nickel-Based Material Vs. 17-22 AS Steel

Sheet-like particles like those seen with Cu-based materials were found. Two different particles were shown in Figure 19. Picture "a" shows the friction surface of a worn particle with the size of 15×10^{-4} meter by 7×10^{-4} meter. Picture "b" gives a close view (1000 $\times$) of the sliding tracks. It is a relatively smooth and dense surface. It is felt a stable and glazy film was formed on the sliding surface which resulted in the high wear resistance especially at higher temperature exposures. Picture "c" shows the failure surface of a particle with the size about 4×10^{-4} meter by 2×10^{-4} meter. Picture "d" indicates the dense structure of the surface layer which was considerably well formed. Also the subsurface was formed before the particle left. Lots of oxides stay on the surface. No further investigation has been carried out for nickel-based material rubbed against 17-22 AS steel.

3) Molybdenum-Based Material Vs. 17-22 AS Steel

A particle with the size of 16×10^{-4} meter by 8×10^{-4} meter is illustrated in Figure 20a. Its smooth friction surface is indicated in Figure 20b with a magnification of 2000. Oxide particles remain on the surfaces, sometimes producing scratches (see low-right of Figure 20c). In Figure 21, attention is given to the cracks along the sliding direction on the friction surfaces. The cracks initiated at the edges and grew inwards. Figure 21b shows the site near the end of the crack. Figure 21d illustrates the source from where the crack started. Next, the edges of the sheet-like particle were examined. Oxide particles appear on all the edges (Figure 22). The edges along the sliding direction show more oxides than the other edges which are across the sliding direction. Therefore, it is felt that the cracks first generate along the sliding direction. The subsurface crack may be

Figure 19 SEM Photographs Showing Two Sheet-Like Particles and their Sliding Surface, Collected from the Tests of Ni-Based Brake Material Sliding Against Steel

× 50

a

× 2000

b

× 2000

c

Figure 20   SEM Photographs Showing a Sheet-Like Particle and its Sliding Surface, Collected from
the Tests of Mo/LPA100 Sliding Against Steel

39.

× 200   c   × 2000   d

× 200   a   × 2000   b
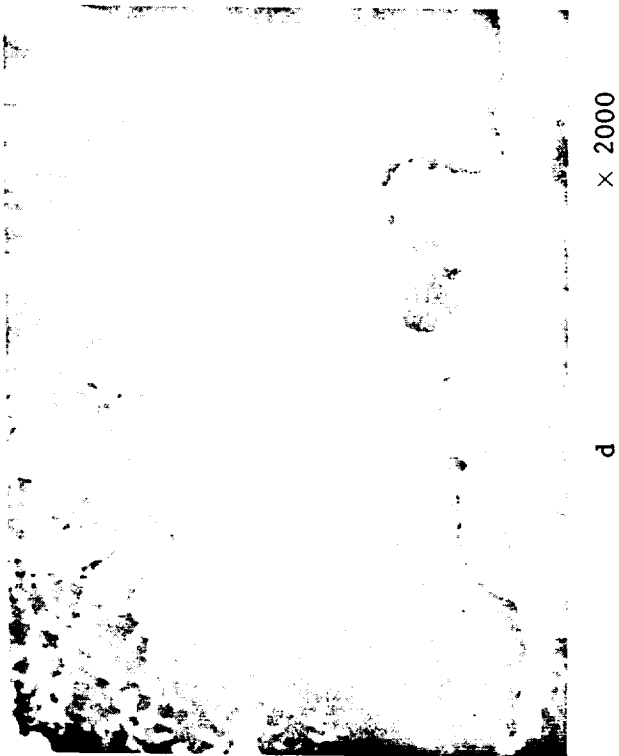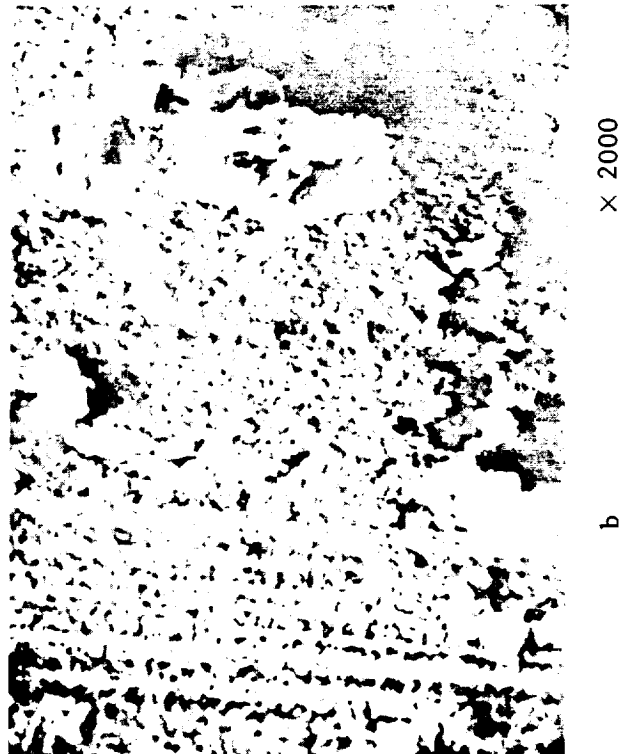
Figure 21   SEM Photographs Showing the Crack Conditions Along the Sliding Direction on the Friction Surfaces of the Same Particle Showing in Figure 20

Figure 22   A Wear Particle of Mo/LPA100 Sliding Against
17-22AS Steel Disc and Its Four Edge Views.

41.

already developed. When the cracks form across the sliding direction the particle will leave as wear debris.

4) Carbon Material Vs. 17-22 AS Steel

The sheet-like particles prevail in this wear debris. Two typical ones with similar size of 5×10^{-4} meter by 4×10^{-4} meter are shown in Figure 23. Picture "a" illustrates the friction surface. Picture "b" indicates at a higher magnification (1000 X) the small piece of particle sticking on the surface. It may be a piece of debris from the steel rotor. It is difficult to find the sliding tracks on the friction surface. Picture "c" shows the failure surface of another particle which is also shown with 1000 magnification in picture "d". It seems that the structure has not been affected by friction. At least it is different from those for the metal based materials rubbed against steel mentioned before. Also Figures 24c and d show the failure surfaces with a crack in picture "c" and lots of oxides in picture "d".

Summary of General Survey of Worn Particles

1. The characteristic shapes of the wear debris under high energy brake performances are sheet-like and very fine powder. It is felt that the very fine debris is formed by abrasion and oxidation together.

2. The sheet-like particle has a facet with friction tracks. The other faces of the particle are the failure surfaces with irregular geometry.

3. The cracks initiate around a large particle (hard abrasive) near the sliding surface.

4. There are three planes along which the cracks can grow. They may grow along the sliding direction due to uneven contact; across the sliding direction due to the frictional stress; or parallel to and below the sliding surface due to material fatigue and oxidation.

5. The oxidation on the surfaces of the crack accelerates the separation.

Figure 23 SEM Photographs Showing a Wear Particle and its Sliding Surfaces, Collected from the Tests of Carbon Sliding Against Steel

43.
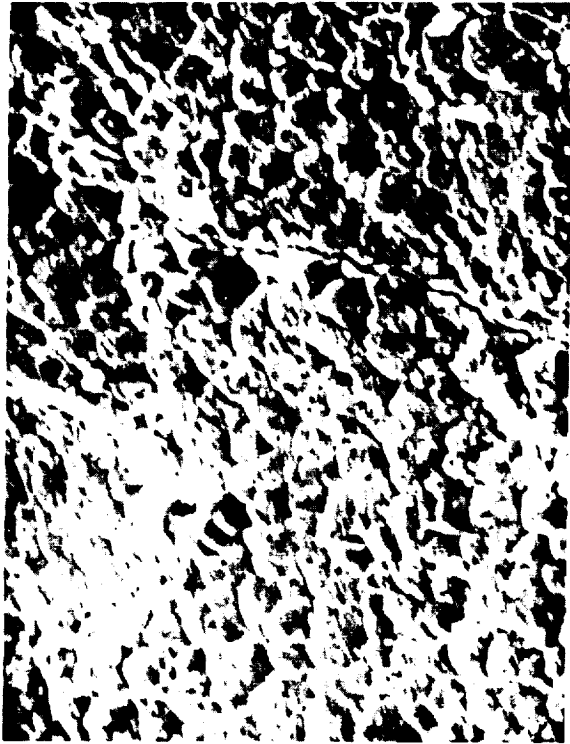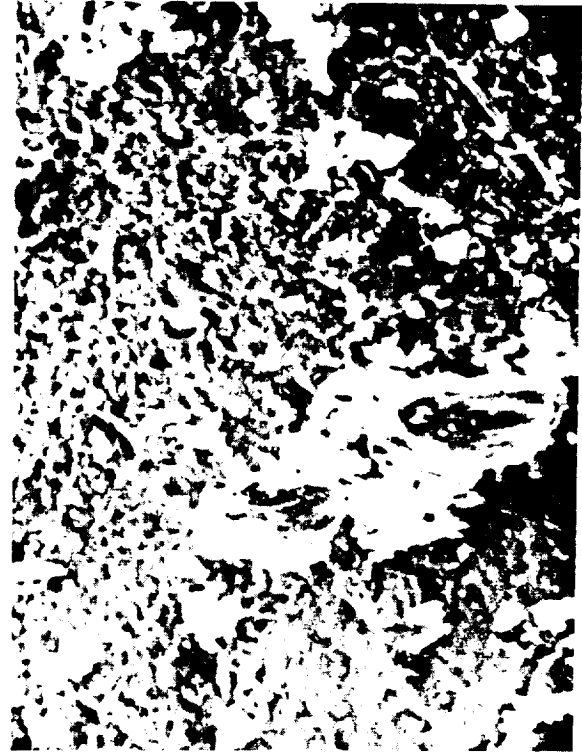
Figure 24   SEM Photographs Showing More Surface Conditions of Wear Particle Collected from Tests of Carbon Sliding Against Steel

6. In general, more oxides appear on the edges along the sliding direction than those on the edges across the sliding direction. Therefore, it is felt that the cracks first penetrate along the sliding direction. The subsurface cracks may be already developed underneath the sliding surface. When the cracks form across the sliding direction the sheet-like particle will be removed.

Effect of Sliding Variables on Wear

This study has been carried out for the case of current copper-based brake material rubbed against 17-22 AS steel. Rig B was used. The velocity was maintained constant at about 1750 rpm for the steel rotor. Three loads, 266.6, 533.2 and 1066.4 N, were applied respectively for three different periods of time, 5, 20 or 60 s. A summary of the results is listed in Table 2.

Several ways were used to express the mutual relations between the factors. Four basic factors were selected as follows:

1. Load

The wear was plotted versus load with the parameter being sliding time (Figure 25a). When sliding time was 5 s or 20 s, the wear is low. Also the change is slight with increase of load. When sliding time is 60 s, the relationship between wear and load is nonlinear. A significant increase of wear takes place under the high load conditions (1066.4 N).

2. Sliding Time

A similar result was obtained when the wear was plotted versus sliding time with the parameter being load (Figure 25b). The wear is not linearly related to slide time when the high load (1066.4 N) is applied for braking.

Also the measured surface temperature was plotted versus sliding time with the parameter being load. Similar curves are obtained for three different loadings. A significant increase takes place at the beginning of sliding. Then the rate of increase of temperature remains relatively constant after sliding for a short period of time (see Figure 26a).

TABLE 2

A SUMMARY OF RESULTS FOR COPPER BASED BRAKE MATERIALS SLIDING AGAINST 17-22 AS STEEL

Time		Load = 266.6 N	533.2 N	1066.4 N
5 s	f_5^*	0.43	0.42	0.37
	ΔW (g)	5.4	6.7	14
	Temp (C)	240	350	530
	CLA**	360	120	110
	Hardness (V)	106	62	50
20 s	f_{20}^*	0.38	0.37	0.39
	ΔW (g)	21	38	140
	Temp (C)	390	550	845
	CLA	200	120	165
	Hardness (V)	50	44	46
60 s	f_{60}^*	0.34	0.33	0.39
	ΔW (g)	49	149	963
	Temp (C)	530	845	1040
	CLA	150	250	200
	Hardness (V)	36	45	29

* f_5, f_{20} or f_{60}: friction coefficient at end of 5, 20 or 60 second sliding, respectively.

** CLA: surface roughness
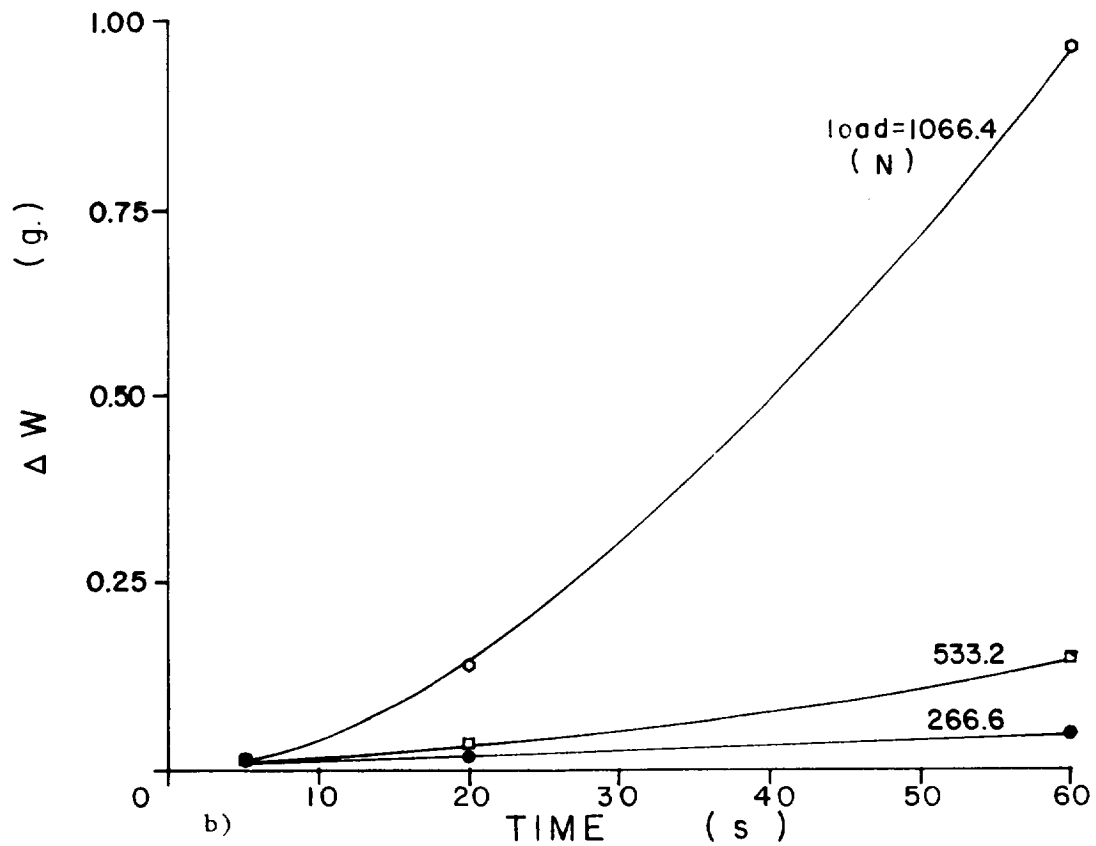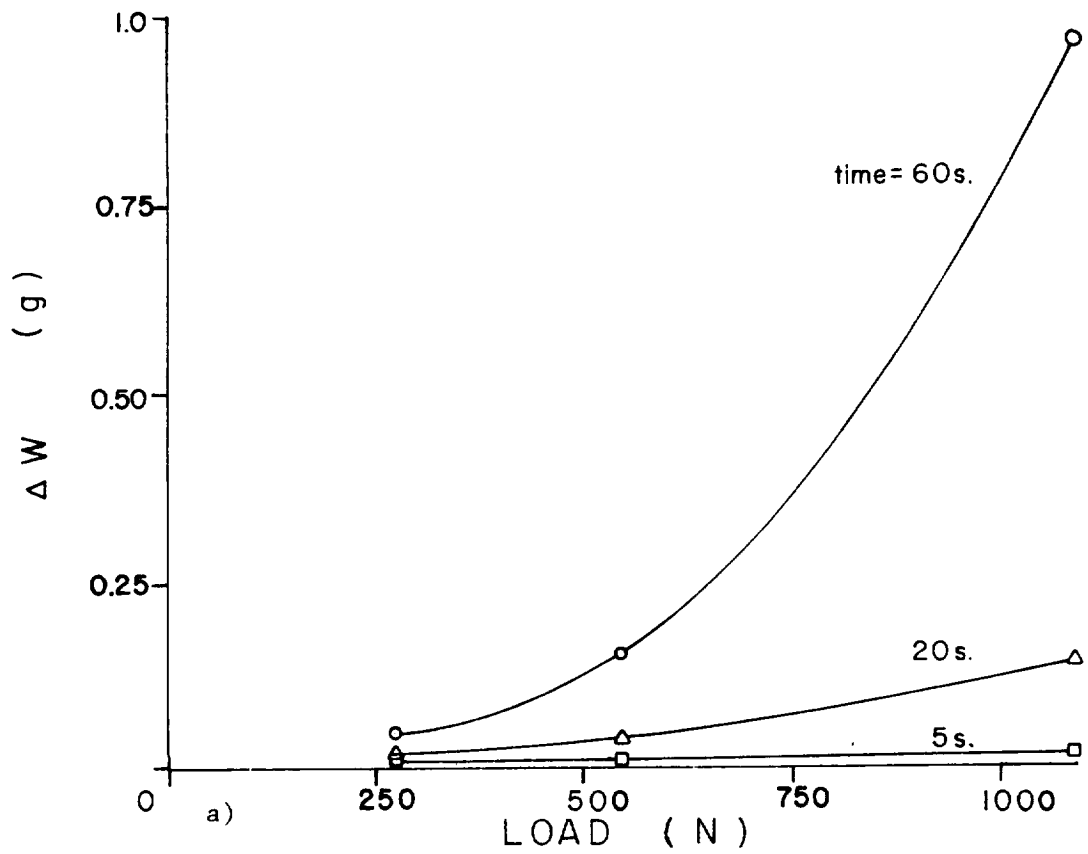
Figure 25   Effects of Load and Slide Time on the Wear of Cu-Based
            Brake Material Rubbed Against Steel

47.
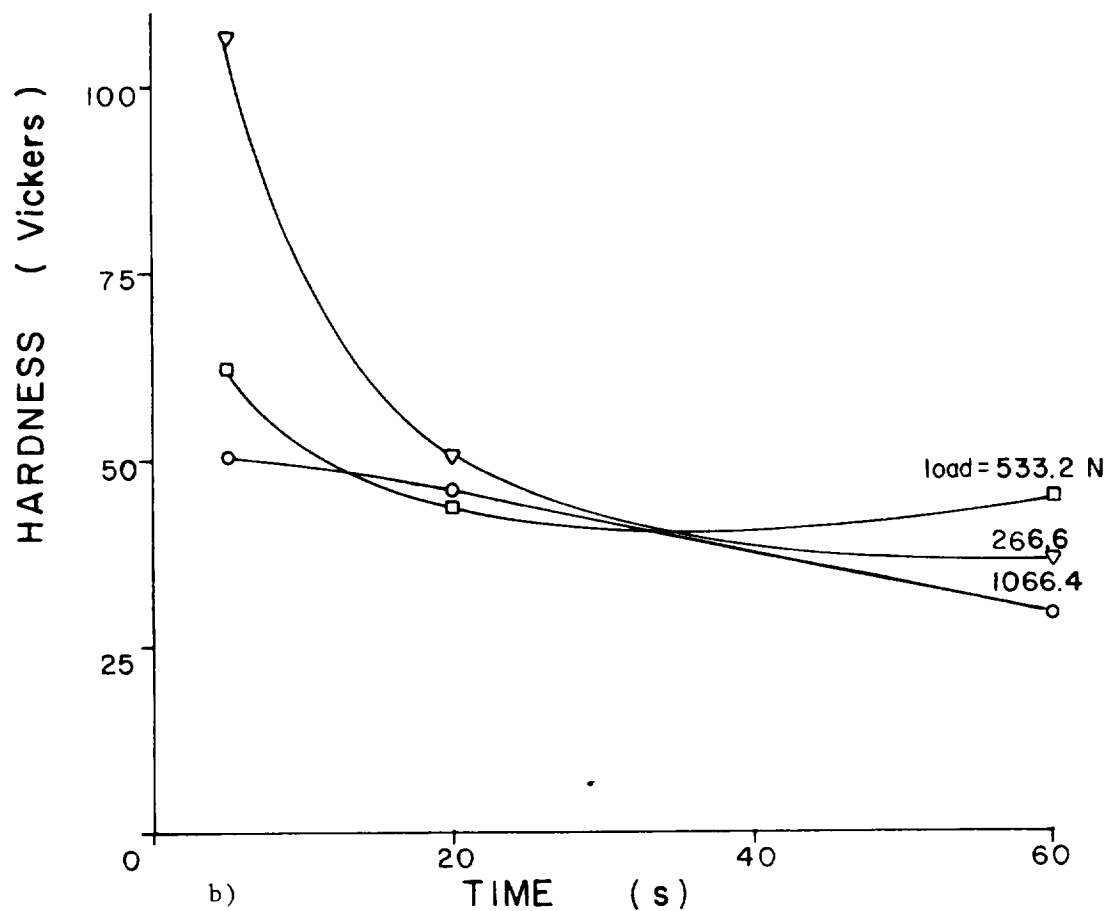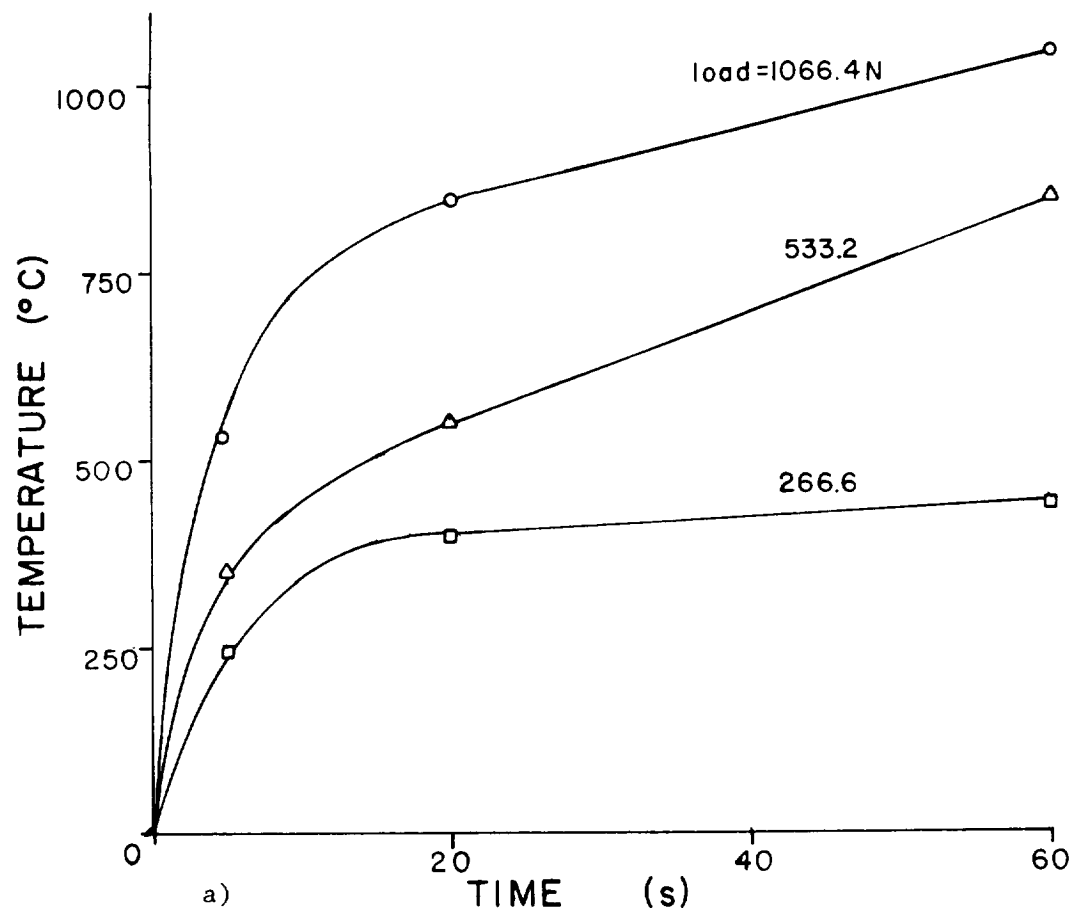
Figure 26 Effect of Sliding Time on the Surface Temperature and Hardness

The hardness of rubbed surface was measured by using a Vickers hardness test machine and its value was plotted versus sliding time for three different load conditions. It is seen that hardness decreases with the time (see Figure 26b).

3. Hardness

The friction was plotted versus final hardness as shown in Figure 27a. The friction increases as the hardness of the rubbed surfaces increases.

Figure 27b shows that the wear is very severe when the final hardness of the rubbed surface is lower than 40 ~ 50 Vickers. It is felt that high temperature which is obtained due to high energy braking softens the slide surface, resulting in the severe wear.

4. Temperature

Hardness was plotted versus the measured surface temperature (Figure 28a). It shows that the frictional heat softens the sliding surface layer. This phenomenon drops the friction (see Figure 28b) and significantly increases the wear (see Figure 29).

It was found that $600^{\circ}C$ (Ref.9) is a critical temperature for current copper-based brake material rubbed against 17-22 AS steel. The wear will increase severely above a surface temperature of $600^{\circ}C$. The melting point of copper is $1083^{\circ}C$. Therefore, when the surface temperature approaches it the material wears drastically.

Based upon an analysis of the relations between the factors in a braking system, it is found that the most representative formula for brake wear is:

1) The near surface temperature (T) is a function of load (L), slide time (t) and velocity (V), i.e.

$$T = f(L, t, V) \tag{A}$$

if velocity keeping constant (V = C), then

$$T = g(L, t) \tag{B}$$
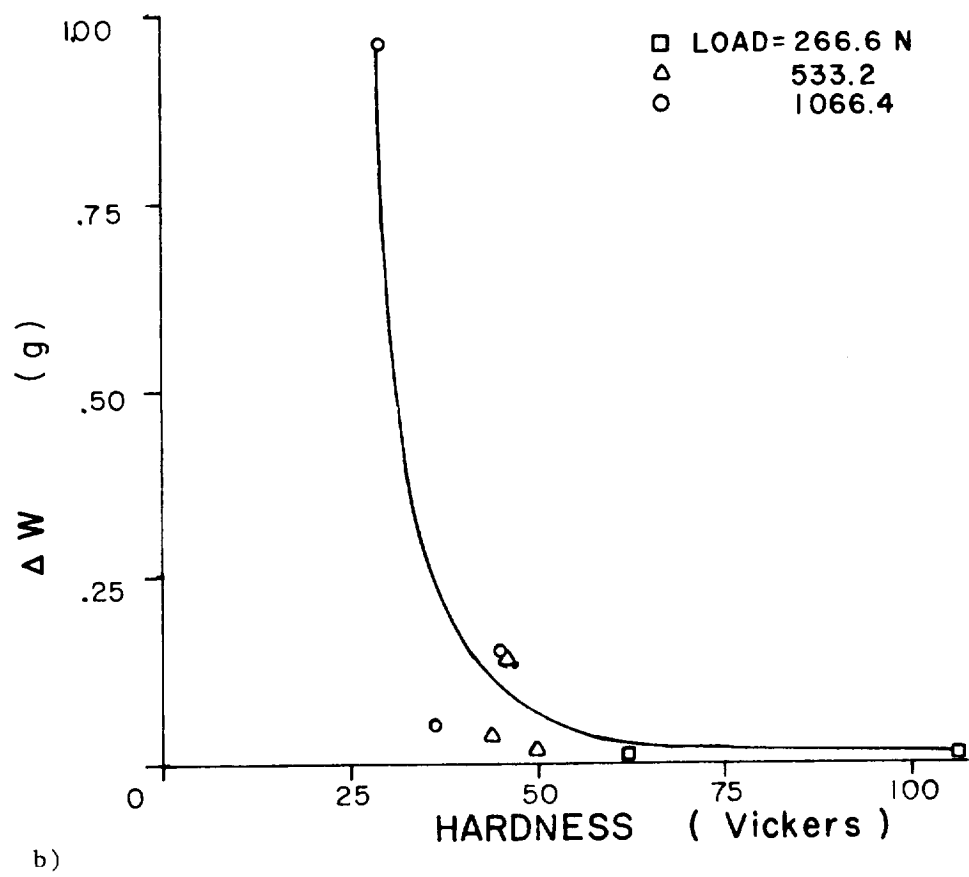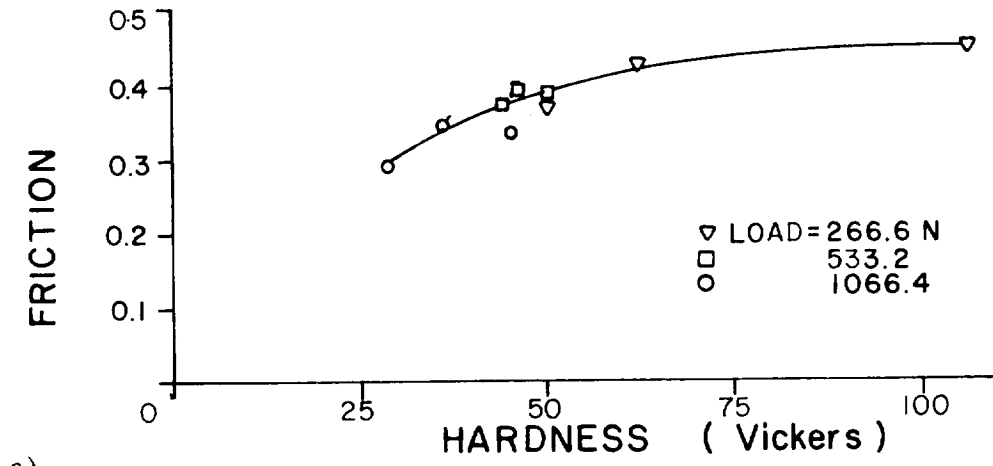
Figure 27   Effect of Hardness on the Friction and Wear Behavior
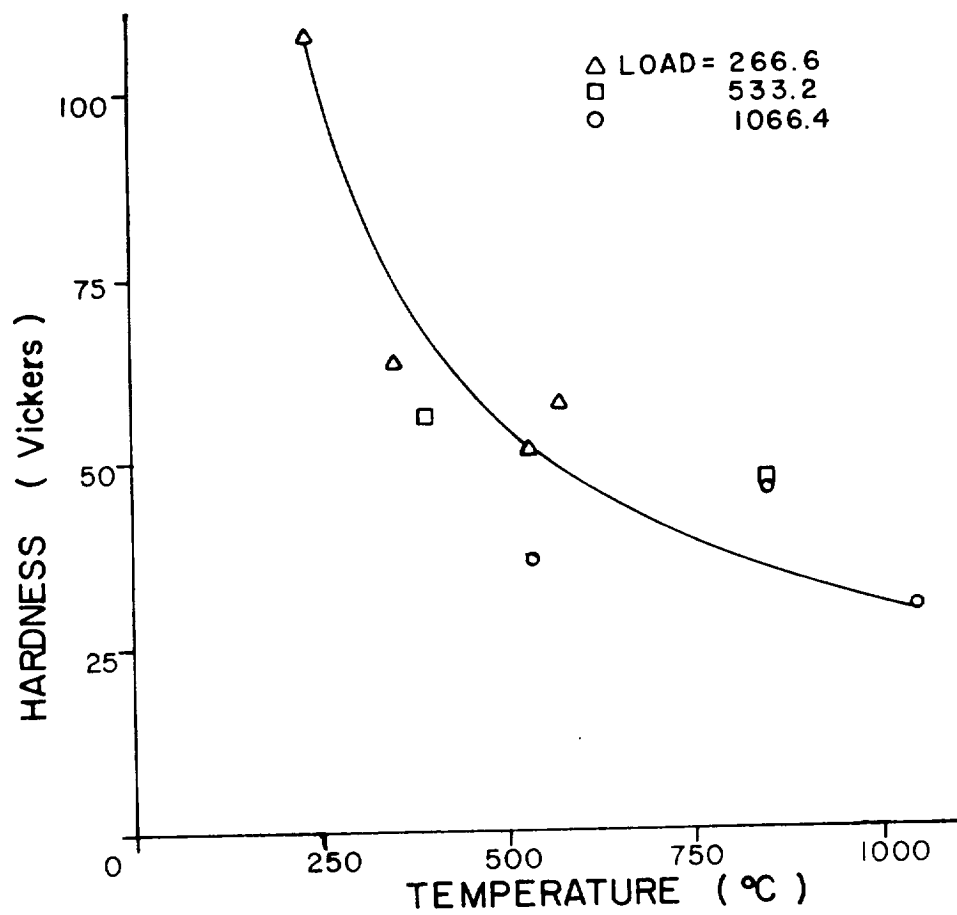
a)
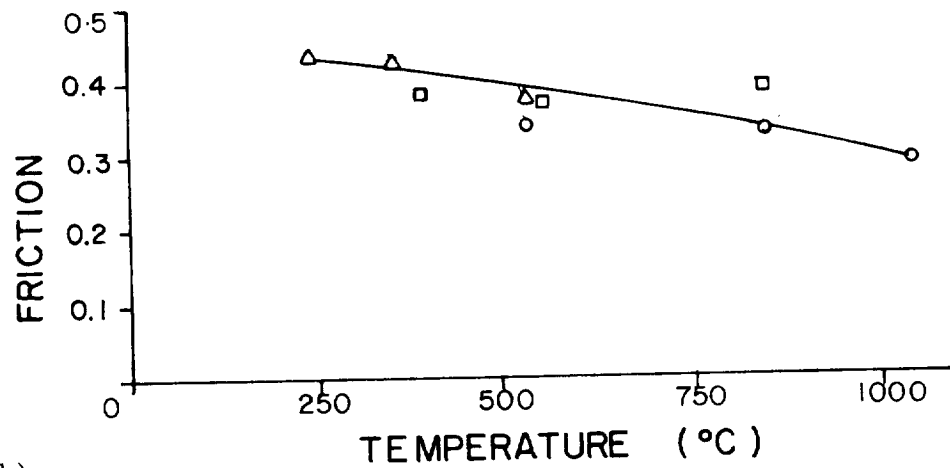
b)

Figure 28   Effect of Surface Temperature on the Hardness and Friction
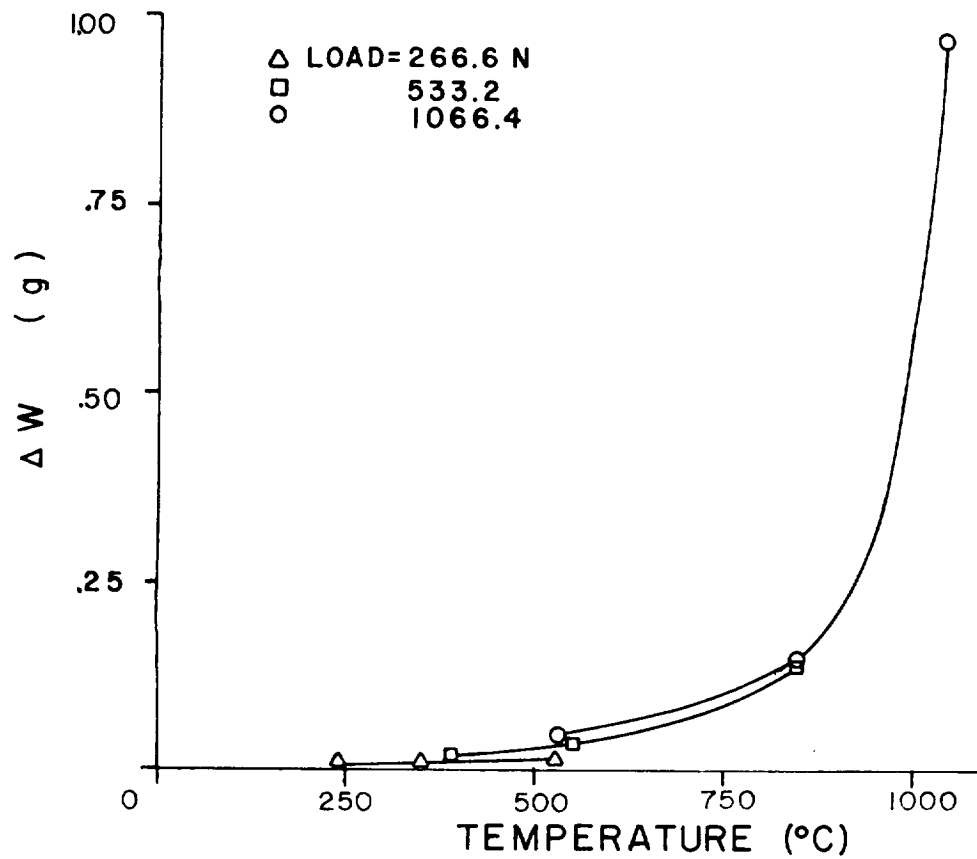
Figure 29   Effect of Surface Temperature on the Wear
of Cu-Based Brake Material Rubbed Against
Steel

2) The wear (ΔW) of the material is then proportional to this temperature, i.e.

$$\Delta W = h(T).$$ (C)

A computer program of "nonlinear least squares" (Ref.18) was applied in order to find a specified function "g" to fit the data values, L, t and T, or a function "h" to fit the data values T and ΔW by means of step-wise Gauss-Newton iterations on some parameters (material constants).

An analogue of creep formula in which the creep strain is a function of stress and time (Ref.19) was by intuition applied in curve fitting of Eq.(B). It yields

$$T = P1 \cdot L^{P2} \cdot t^{P3}$$ (D)

where P1, P2 and P3 are parameters. It has been found that when

$$P_1 = 9.1$$
$$P_2 = 0.5$$ (E)
$$P_3 = 0.3$$

with load (L) in N, time (t) in s, and near surface temperature (T) in $^\circ$C, Eq.(D) will most fit the experimental points (Table 2). Use of the Cal-comp plotter basic software package (Ref.20) has been employed in plotting the equation and experimental data together for easy comparison. It is shown in Figure 30. It shows that the near surface temperature increases due to friction is neither linearly proportional to sliding time or to the load. The problem is that the equation (D) is not derived on the basis of some mathematical model. It is difficult to interpret P_1, P_2 and P_3 physically now. But the equation is in a simple form to predict the surface temperature of lining materials during the friction process in a specific brake system.

The melting point of copper was emphasized in the curve fitting by using the equation (C). Therefore it becomes

$$\Delta W = K \cdot \frac{T}{T^* - T}$$ (F)
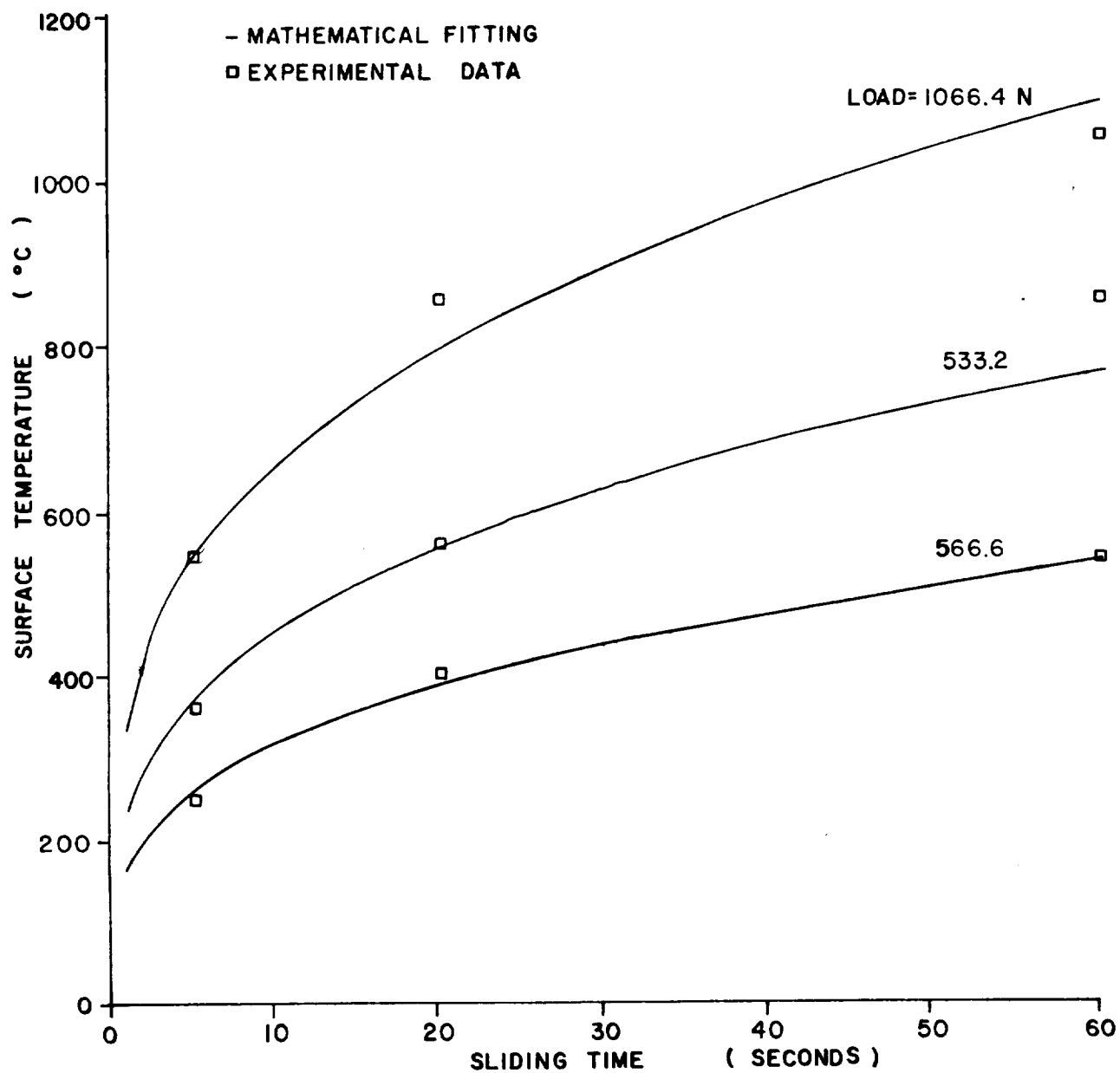
Figure 30 Effect of Sliding Time and Load on Surface Temperature of Cu-Based Brake Material Rubbed Against Steel

where K is constant, T^* is the melting point of copper (= 1083°C). When K = 39.785, Eq.(F) was plotted in Figure 31 with the experimental points. The matching means that the softening of base metal is a dominant factor in the whole wear process. In other words, the base matrix of higher melting point will give better wear behavior especially at high temperature range. Although this simple formulation may be argued in many ways, it is a tool that will be applied in the later interpretation of the wear mechanism of current aircraft brakes. The most interesting point to note is that a smooth curve describes the wear behavior from relatively low temperatures up to the melting point. This can indicate that the softening process, which becomes excessive near the melting point, operates throughout the whole temperature range.

It is seen that the wear process of current aircraft brake materials is dominated by a melting mechanism of copper matrix. The wear debris formation as a result of the joining of cracks which occur in the surface layer is dependent upon the stress field applied. It is also controlled by the frictional heat generated which raises the contact temperature even near the melting point of metallic matrix locally. Weakness of this matrix bond speeds the crack growth. Therefore the wear mechanism developed is essentially a temperature dependency.
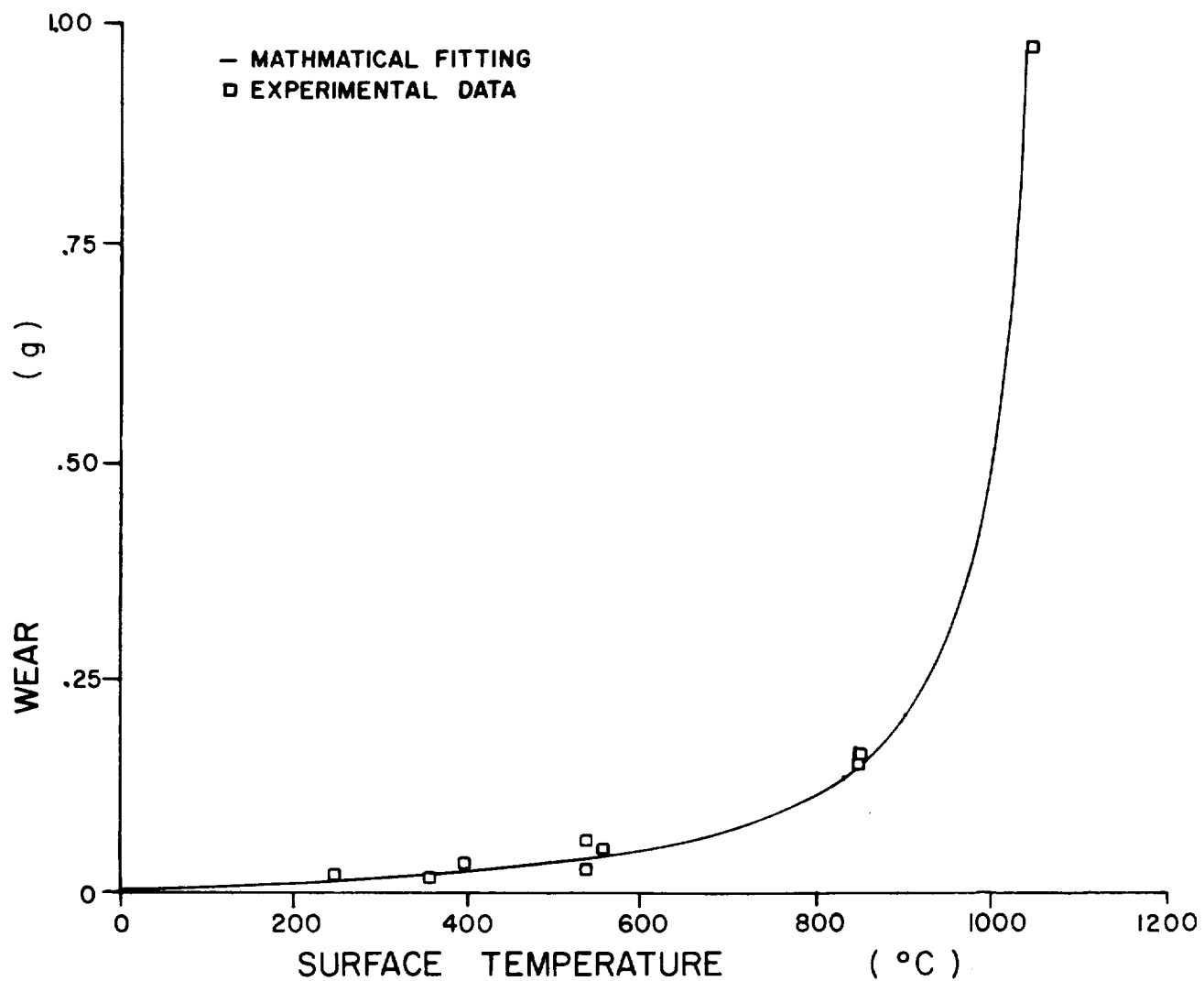
Figure **31** Effect of Surface Temperature on the Wear of Cu-Based
Brake Material Sliding Against 17-22 AS Steel

Proposed Model of Wear Behavior

Based upon the previous work a wear model (see Figure 32) can be proposed for the current copper-based brake material. Essentially this model proposes that cracks are formed in the surface layer of the brake material due to the variations in the normal and frictional stresses. These cracks are either perpendicular to the sliding surface or parallel (subsurface cracks). The critical cracks are the subsurface ones which initiate at a hard particle inclusion and allow particles to be removed by intersecting the cracks perpendicular to the surface. Since the wear is proportional to temperature the cracks propagate by a ductile fracture phenomenon accelerated by oxidation. This model is described in more detail in the following paragraphs.

1) Material Transfer. An appreciable amount of iron is transferred from the steel rotor to the pads because of adhesion during high temperature sliding. This iron transfer affects the structure of sliding surface layer. No notable amount of copper or copper oxide was found on the worn surfaces of the steel rotor.

2) Oxidation. The actual oxide film thickness (h) as measured on a large number of used pads is about 4.0×10^{-6} meter (0.00016") (Ref.8). But at a depth (shown in Figure 32 as H) of 4.8×10^{-4} meter (0.019") below the sliding surface, copper oxide (Cu_2O) and iron oxides were still detected by X-ray.

3) Particle. Primarily the wear debris is metallic and heavily oxidized. In general the wear consisted of flat plates of average size about 4.0×10^{-4} meter $\times 3.0 \times 10^{-4} \times 0.3 \times 10^{-4}$. This means the thickness of the plate is larger than that of the oxide film (h) but less than the depth (H) where the oxides were still detectable by X-ray. In other words, the severe wear mechanism during high temperature sliding is not simply the removal of thin heavily oxidized film. The cracks generated in the surface layer mainly cause the severe wear. It is felt the oxidation accelerates this process forming the wear particles.
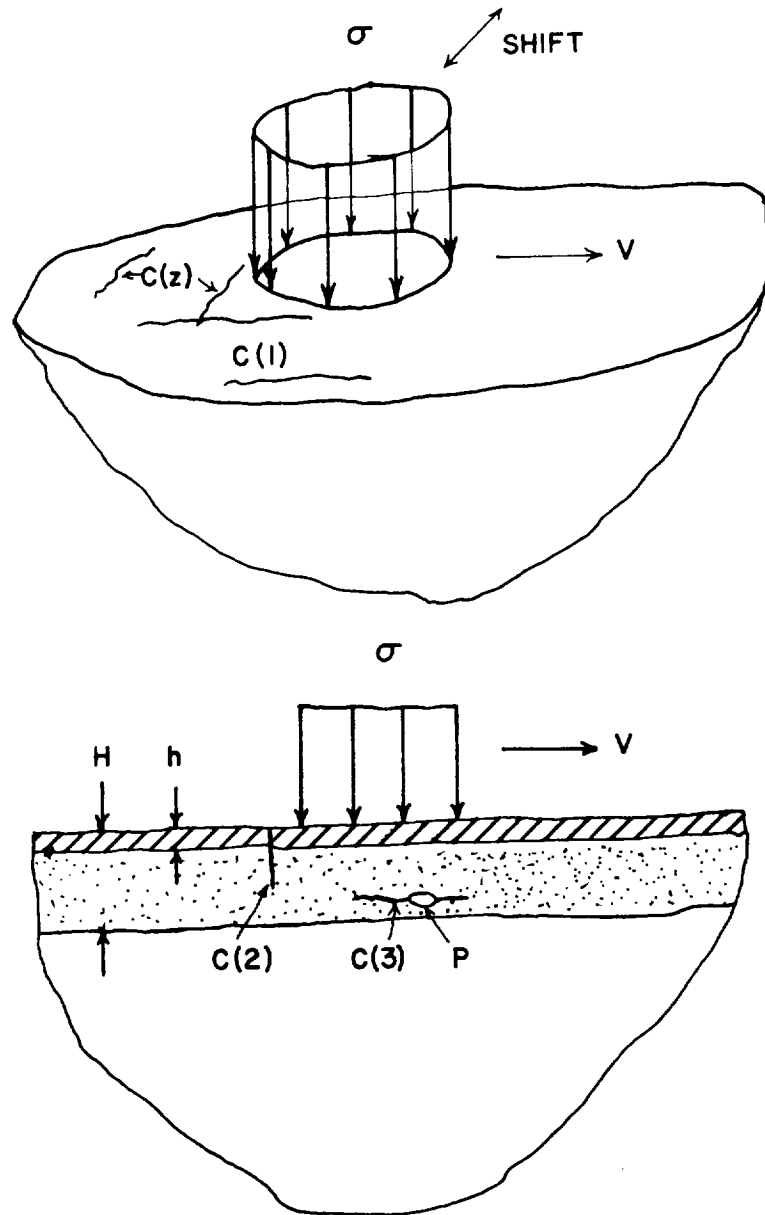
V: Velocity of sliding
σ: Local loading (it shifts)
h: Oxide film thickness $\cong 4.0 \times 10^{-6}$ meter (0.00016")
H: Depth oxide detected by X-ray $\cong 4.8 \times 10^{-4}$ meter (0.019")
P: Large particle (abrasive)
C(1): Crack (1), along sliding direction
C(2): Crack (2), cross sliding direction
C(3): Crack (3), subsurface crack.

Figure 32   Proposed Wear Model

4) Loading Shift. The local loading stress is designated as σ in Figure 32. It is a function of time and location. It was mentioned before that this loading shifts due to the "Barber Effect" which is a problem of the thermoelastic and thermoplastic instabilities in sliding. All these mechanical and thermal disturbances will result in the cracks on the sliding surface layer (labelled as "C(1)" in Figure 32).

5) Shear Stress. The frictional force initiates the cracks [C(2)] across the sliding direction due to the tensile stress in the surface layers.

6) Fatigue. In Figure 32, "P" stands for a relatively large particle imbedded in the surface layer. This particle initiates a third kind of crack [C(3)]. Under the combination of applied loading stress and shear stress, both of which are randomly periodic, the crack propagates to form a subsurface crack, parallel to and below the sliding surface. The oxidation accelerates this separation. These three direction cracks [C(1), (2) and (3)] allow the wear particles to leave.

7) Temperature. The surface temperature is nonlinearly proportional to sliding time and applied load with constant speed, i.e.

$$T = 9.1 \ L^{0.5} \ t^{0.3}.$$

The frictional heat lowers the yield strength of the base matrix (copper). Therefore the total wear is a function of temperature. Also the melting point ($T^{*} = 1083^{\circ}C$) is introduced in the formula, i.e.

$$\Delta W \cong 40 \ \frac{T}{T^{*} - T} \ .$$

This softening is in other words, related to the fatigue constant which accelerates the crack growth. Therefore, the wear model proposed here is primarily surface temperature dependent.

Comments

The inhomogeneity and porosity of the current copper based brake materials which are fabricated by the power metallurgical methods have to be considered before further discussion. Therefore, the recrystallization theory of wear (Refs.1 and 2) would not be applicable to cover the wear processes of these

materials totally. However, the recrystallization of the copper matrix would not be neglected in the high temperature sliding. The tests are needed to prove this point. Also the depth extent to which the material is recrystallized by frictional heat is a temperature dependency. This may be related to the penetration of heavy oxidation from the sliding surface.

The formation of the "sheet-like" wear particles under the high energy braking was found mostly in agreement with the wear mechanism of "delamination" established by Suh (Refs.3 and 4). Especially, the three sense cracks are initiated and propagated under a tension-compression field, then merge to allow the wear particles worn away. This stress field is randomly cyclic because of the instability of sliding (Ref.17), particularly at high temperatures (Refs.21 and 22). Dislocations have not been mentioned by the author here. The crack nucleation occurring around a large particle embedded near the surface and the intergranular cracking sound much more reasonable for the porous lining materials. The cracking would propagate easily by merging the voids deformed due to friction. All these have been represented by a simple temperature formula which fits the experimental data almost covering all operative ranges of copper matrix. Indeed, this investigation is just a beginning. Further work is needed to formulate a sophisticated phenomenological wear mechanism.

SECTION 6

SUMMARY OF RESULTS

A study has been conducted concerning the wear and sliding character-
istics of brake materials using various surface analysis and mathematical
techniques. Based upon observation of the surfaces of the frictional ma-
terials and the rotor steel and upon the examination of the worn particles,
two dominating factors, oxidation and heat softening dominate the wear be-
havior of the brake material. The following specific results have been ob-
tained in this investigation.

1) Wear particles are of a similar shape and size regardless of the
   operating conditions under which they are formed.

2) The wear particles are generally platelets with one large face being
   the sliding surface. The other faces are fracture surfaces.

3) The fracture of film was studied for current copper based brake ma-
   terial rubbed against 17-22 AS steel. The surface cracks initiate
   around a site of a hard and relatively large particle (may be abras-
   ive) embedded near the sliding surface.

4) There are three planes along which the cracks grow. They may grow
   along the sliding direction. This growth results mainly from the
   "Barber effect" which is a problem of thermoelastic and thermoplastic
   instabilities in sliding due to uneven contact. The mechanical and
   thermal disturbances will cause the cracking growth on the sliding
   surface layer. The frictional stresses initiate cracks across the
   sliding direction. The third kind of crack grows parallel to and
   below the sliding surface to form a "subsurface." This results from
   the material fatigue or weakness of bond between the surface film
   and its substrate. Oxidation accelerates this separation.

5) The surface temperature was related to the braking variables,
   velocity (V), load (L) and slide time (t). Keeping velocity constant,
   the equation was found:

$$T = P_1 \cdot L^{P2} \cdot t^{P3}$$

where

$$P_1 = 9.1$$
$$P_2 = 0.5$$
$$P_3 = 0.3$$

This fits the experimental data. It means that the surface temperature is nonlinearly proportional not only to load but also to sliding time.

6) It was found that the wear behavior of this current brake material is dominated by a copper softening phenomenon in the whole operative temperature range up to melting point. A simple equation yields

$$W = K \cdot \frac{T}{T^* - T} \cong 40 \cdot \frac{T}{1083 - T}$$

where $K = 39.785$ and $T^* =$ melting point of copper and $T =$ operative temperature .

7) This formulation of wear behavior in terms of surface temperature confirms what has been found in microscopical studies. The surface temperature affects the oxidation rate, the film stability and the strength of base metal matrix. All of these determine the wear behavior.

REFERENCES

1. R.C. Bill and D. Wisander, "Role of Plastic Deformation in Wear of Copper 10-Percent-Aluminum Alloy in Cryogenic Fuels," NASA TN D-7253, 1973.

2. R.C. Bill and D.W. Wisander, "Surface Recrystallization Theory of the Wear of Copper in Liquid Methane," NASA TN D-7840, 1974.

3. N.P. Suh, "The Delamination Theory of Wear," Wear, Vol.25, pp.111-124, 1973.

4. N.P. Suh, S. Jahanmir, J. Fleming, E.P. Abrahamson, II, N. Saka and J.P. Teixeira, "The Delamination Theory of Wear - II," Progress Report to the Advanced Research Project Agency, DOT No. N00014-67-A-0204-0080, NR 229-011, 1975.

5. H. Koba and N.H. Cook, "Wear Particle Formation Mechanisms," Final Report to the Office of Naval Research, No. N00014-67-A-0204-0054, NR 229-003, 1974.

6. V.C. Westcott, D. Scott, J.L. Middleton and R.A. White, "Studies of the Nature of Wear," Technical Report to the Advanced Research Project Agency, ARPA No. 2532, 1974.

7. V.C. Westcott and J.L. Middleton, "The Investigation and Interpretation of the Nature of Wear Particles," Final Report to the Office of Naval Research, No. N00014-73-C-0455, NR 229-005, 1974.

8. M.B. Peterson and T.L. Ho, "Consideration of Materials for Aircraft Brakes," NASA CR-121116, 1972.

9. T.L. Ho and M.B. Peterson, "Development of Aircraft Brake Materials," NASA CR-134663, 1974.

10. T.L. Ho, F.E. Kennedy and M.B. Peterson, "Evaluation of Materials and Design Modifications for Aircraft Brakes," NASA CR-134896, 1975.

11. T.L. Ho and M.B. Peterson, "Frictional Characteristics of the Nickel-Based Brake Materials Sliding Against 17-22 AS Steel," Project Technical Report (to be submitted).

12. U. Valdre, "Electron Microscopy in Material Science," Academic Press, 1971.

13. N.A. Hooton, "Metal Ceramic Composites in High Energy Friction Application," Bendix Technical Journal, Vol.2, No.1, 1969.

14. B.D. Cullity, "Elements of X-Ray Diffraction," Addison-Wesley, 1967.

15. O. Kubaschewski and B.E. Hopkins, "Oxidation of Metals and Alloys," Academic Press, 1962.

16. K. Hauffe, "Oxidation of Metals," Plenum Press, New York, 1965.

17. J.R. Barbar, "Thermoelastic Instabilities in the Sliding of Conforming Solids," Proc. Roy. Soc., A, Vol.312, pp.381-394, 1969.

18. BMDX85, "Nonlinear Least Squares."

19. J.A.H. Hult, "Creep in Engineering Structures," Blaisnell Publishing Company, 1966.

20. A. Larsen, "Calcomp Plotter Basic Software," RPI Technical Publication, 1975.

21. F.E. Kennedy, J.J. Wu and F.F. Ling, "A Thermal Thermoelastic and Wear Analysis of High-Energy Disk Brakes," NASA CR-134507, 1974.

22. J.J. Santini, "Effect of Design Factors on Surface Temperature and Wear in Disk Brakes," NASA CR-134923, 1976.

I. AIR FORCE   Number of Copies

    A. AFFDL
        Wright-Patterson AFB, OH   45433

        1. FEM/Ken H. Digges   .1
        2. FE/T. J. Baker   1
        3. Library   1
        4. Code FBE   1

    B. AFML/MX
        Wright-Patterson AFB, OH   45433   1

    C. AF Office of Scientific Research
        Aeromechanics and Energetics Division
        Arlington, VA   22209   1

    D. USAF
        Directorate of Aerospace Safety
        Norton Air Force Base, CA   92409   1

II. ARMY

    A. Commanding Officer
        US Army Air Mobility and Development Laboratory
        Fort Eustis, VA   23604

        1. Library   1

    B. US Army Agency for Aviation Safety
        Fort Rucker, AL   36360   1

    C. Commanding Officer
        US Army Materials and Mechanics Research Center
        Watertown, MA   02172

        1. AMXMR-ED   1

III. <u>DOD</u>   <u>Number of Copies</u>

    A. Defense Documentation Center
       Cameron Station
       Alexandria, VA 22314

       1. Library   1

IV. <u>FAA</u>

    A. Federal Aviation Administration
       800 Independence Avenue, S. W.
       Washington, DC 20591

       1. Library   1
       2. Gustav E. Lundquist, Code AED-1   2
       3. Robert Auburn, Code AFS-140   1
       4. Herbert H. Slaughter, Code AFS-100   1
       5. James F. Rudolph, Code AFS-1   1

    B. Federal Aviation Administration
       400 Seventh Street, S. W.
       Washington, DC 20590

       1. Phil Bolger   1

V. <u>NASA</u>

    A. National Aeronautics and Space Administration
       Washington, DC 20546

       1. John H. Enders, Code ROO   1
       2. Kenneth E. Hodge, Code RO   1
       3. R. Prichard, Code DB   1
       4. George W. Cherry, Code RD-P   1

    B. NASA Ames Research Center
      Moffett Field, CA 94035

       1. Library   1
       2. Bradford H. Wick   1
       3. William J. Gilwer, Jr.   1

		Number of Copies
C.	NASA Flight Research Center P.O. Box 273 Edwards, CA 93523	
	1. Library	1
	2. Stanley P. Butchart	1
	3. Elmor J. Adkins	1
D.	NASA Langley Research Center Hampton, VA 23665	
	1. Library	1
	2. R. W. Boswinkle, Jr., MS 116	1
	3. J. W. Stickle, MS 246A	1
	4. J. A. Zalovcik, MS 247	1
	5. J. L. McCarty, MS 497	1
E.	NASA Lewis Research Center 21000 Brookpark Road Cleveland, OH 44135	
	1. Solomon Weiss, MS 500-318	3
	2. Lawrence P. Ludwig, MS 23-2	1
	3. Robert C. Bill, MS 23-2	1
	4. James H. Zimmerman, MS 500-302	1
	5. Library, MS 60-3	2
	6. Report Control Office, MS 5-5	1
	7. Technology Utilization, MS 3-19	1
	8. William H. Swann, MS 4-8	1
	9. Donald Petrash, MS 500-204	6
	10. Harold W. Schmidt, MS 500-318	5
F.	NASA Lyndon B. Johnson Space Center Houston, TX 77058	
	1. Library	1
	2. Joseph S. Algranti, Code CC	1
G.	NASA Scientific and Technical Information Facility P. O. Box 33 College Park, MD 20740	6
H.	National Technical Information Service (Department of Commerce) Springfield, VA 22151	6

4

Number of Copies

VI.

    A. National Aviation Facilities Experimental Center
        Atlantic City, NJ 08405

        1. Library   1
        2. George Bates   1

VII. NTSB

    A. National Transportation Safety Board
        800 Independence Avenue, S. W.
        Washington, DC 20591

        1. Martyn V. Clarke, Code BAS-10   2
        2. Library   1

VIII. NAVY

    A. Naval Air Propulsion Test Center
        Trenton, NJ 08628

        1. Library   1

    B. Commanding Officer
        Naval Aviation Safety Center
        Norfolk, VA 23511   1

    C. Naval Research Laboratory
        Washington, DC 20390

        1. Library, Code 2029   1

    D. Office of Naval Research
        Washington, DC 20360

        1. Library   1

IX. Aircraft Industry/Consultants/Industrial Organizations

    A. Aeronautical Research Associates of Princeton
        50 Washington Road
        Princeton, NJ 08540

        1. J. C. Houbolt   1

B. Air Line Pilots Association
    1625 Massachusetts Avenue, N. W.
    Washington, DC   20036

    1. Theodore G. Linnert   1

C. Air Transport Association
    Washington, DC   20036

    1. Clifton F. Von Kann   1

D. Aircraft Owners and Pilots Association
    4650 East-West Highway
    Bethesda, MD   20014

    1. Michael V. Huck   1

E. Abex Corporation
    Friction Products Group
    5372 W. 130 Street
    Cleveland, OH   44142

    1. Robert Shaw   1

F. American Airlines, Incorporated
    633 Third Avenue
    New York, NY   10017

    1. Franklin W. Kolk   1

G. Battelle Memorial Institute
    505 King Avenue
    Columbus, OH   43201

    1. Library   1

H. Beech Aircraft Corporation
    Wichita, KS   67201

    1. G. S. McCormick   1
    2. M. O'Connor   1

I. Bell Aerospace Company
    Box 1
    Buffalo, NY   14240

    1. Director of Safety   1

J. The Boeing Company
    Commercial Airplane Group
    P.O. Box 3707
    Renton, WA 98124

    1. William H. Cook   1

K. Continental Aviation and Engineering Corporation
    12700 Kercheval Avenue
    Detroit, MI 48215

    1. Technical Library   1

L. Douglas Aircraft Company
    3855 Lakewood Boulevard
    Long Beach, CA 90801

    1. Technical Library   1

M. Flight Safety Foundation, Incorporated
    1800 North Kent Street
    Arlington, VA 22209

    1. Jerome Lederer   1

N. General Dynamics Corporation
    Box 1128
    San Diego, CA 92112

    1. Director of Safety   1

O. General Motors Corporation
    Materials and Structures Laboratory
    Warren, MI 48090   1

P. B. F. Goodrich Corporation
    Department 8531
    9921 Brecksville Road
    Brecksville, OH 44141

    1. Edward Tatarzycki   1

Q. Goodyear Aerospace Corporation
1210 Massillon Road
Akron, OH 44315

   1. Mr. R. R. Wiseman   1

R. Grumman Aerospace Corporation
South Oyster Bay Road
Bethpage, NY 11714

   1. Director of Safety   1

S. Lockheed-California Company
Burbank, CA 91503

   1. E. J. Versaw   1
   2. Technical Library   1

T. McDonnell Douglas Corporation
Box 516
St. Louis, MO 63166

   1. Director of Safety   1

U. Northrop Corporation
Aircraft Division
3901 West Broadway
Hawthorne, CA 90250

   1. Technical Library   1

V. Pan American World Airways
Building 208
JFK International Airport
Jamaica, NY 11430

   1. John G. Borger   1

W. Piedmont Aviation, Incorporated
Smith Reynolds Airport
Winston-Salem, NC 27102

   1. William M. Magruder   1

X. Mr. I. Irving Pinkel
    4671 W. 210 Street
    Fairview Park, OH 44126   1

Y. Trans World Airlines, Incorporated
    605 Third Avenue
    New York, NY 10016

    1. Robert W. Rummel   1

Z. United Airlines, Incorporated
    P.O. Box 66100
    Chicago, IL 60666

    1. Lloyd L. Treece   1

X. UNIVERSITIES

    A. Boston University
        Department of Aerospace Engineering
        110 Cummington Street
        Boston, MA 02215

        1. Ming M. Chen   1

    B. The City College of the University of New York
        Department of Mechanical Engineering
        New York, NY 10031

        1. S. B. Menkes   1

    C. The Johns Hopkins University
        Applied Physics Laboratory
        8621 Georgia Avenue
        Silver Spring, MD 20910

        1. Gordon L. Dugger   1

    D. Massachusetts Institute of Technology
        Cambridge, MA 02139

        1. Emmett A. Witmer, 41-219   6
        2. Robert Simpson   1

9

E. The Pennsylvania State University
    Department of Aerospace Engineering
    233 Hammond Building
    University Park, PA   16802

    1. B. W. McCormick   1

F. Rensselaer Polytechnic Institute
    Troy, NY   12181

    1. (F. F. Ling will decide number for distribution)

G. Texas A & M University
    Department of Aerospace Engineering
    College Station, TX   77843

    1. J. A. Stricklin, Jr.   1

H. University of California
    Department of Civil Engineering
    Berkeley, CA   94720

    1. Robert Haronjeff   1
    2. V. F. Zackay   1

I. University of Illinois
    711 Glasgow Street (Apt. 1)
    Inglewood, CA   90301

    1. Stanley W. Roscoe   1

J. The University of Michigan
    Ann Arbor, MI   48105

    1. Samuel K. Clark   2

K. University of Notre Dame
    Department of Aeromechanical Engineering
    Notre Dame, IN   46556

    1. L. H. N. Lee   1

L. University of West Virginia
    College of Engineering
    Morgantown, WV   26505

    1. J. B. Fanucci   1

M. Northwestern University
Department of Mechanical Engineering
and Astronautical Sciences
619 Clark Street
Evanston, IL 60201

    1. Ralph A. Burton   1

XI. Additions to Aircraft Industry, etc. (IX)

A. Bendix Corporation
Energy Controls Division
717 North Bendix Drive
South Bend, IN 46620

    1. Robert W. Moore, Military Applications Manager   1
    2. Douglas Roth, Engineering Manager   1

B. Bendix Corporation
Friction Material Engineering
Troy, NY 12181

    1. W.G. Urso, Project Engineer   1

C. Bendix Research Laboratory
Southfield, MI 48076

    1. Seong K. Rhee   1
    2. W. Spurgeon   1

D. Cessna Aircraft Company
Aircraft Marketing
580 Pawnee Road
Wichita, KS 67218

    1. Bernard W. Bogard, Manager   1

E. E.I. DuPont de Nemours & Company, Inc.
Petroleum Chemicals Division
Tribaloy Products
Glasgow Site
Wilmington, DE 19898

    1. Curtis Cameron   1

Number of Copies

F. Goodyear Aerospace Corporation
P.O. Box 9023
Akron, OH 44315

   1. Edward Aukscunas   1
   2. Fred Kirkhart   1
   3. John Nelson   1

G. International Nickel Company, Inc.
One New York Plaza
New York, NY 10004   1

H. Pure Carbon Company, Inc.
St. Mary's, PA 15857

   1. Thomas Ormiston   1

I. B.F. Goodrich Engineering Systems Company
Wheel and Brake Plant
Troy, Ohio 45373

   1. Vijay Rastogi, Manager   1
       Materials & Technology